CENTRO DE INVESTIGACIONES EN ÓPTICA, A.C.

Surface Enhanced Raman Substrate Design: Probe On Organic Dyes And Pesticides.

Dissertation submitted as a partial fulfillment of the requeriments for the degree of Doctor in Science (Optics) at Centro de Investigaciones en Óptica

Student: Mónica Monserrat Martínez García

Advisor: Juan Luis Pichardo Molina

October, 2018
León, Guanajuato, México

Final edition. Includes changes suggested by reviewers.

Abstract

The aim of this work is the design, development and preparation of an efficient SERS substrate for the detection at low concentrations of dyes and pesticides.

Concave gold nanocubes (CGNC) were synthesized by chemical reduction method, and were characterized by UV-Vis spectroscopy and by scanning electron microscopy (SEM), to ensure the proper morphology and size.

An aluminum alloy (*Al-6063*) base was used for the nanoparticle deposit, since it does nor present Raman signal that could opaque the response signal of the analyte of probe. The surface of the slides was modified, first by mechanical treatment and then, were subjected to an electropolish process. Later were functionalized with silane molecules. The surface substrates was characterized by atomic force microscopy (AFM) and by X-ray diffraction (XRD), to confirm the presence of pseudoboehmite in the surface.

In order to select the size of nanocube that showed the best Raman signal improvement, solutions of nanoparticles of different sizes ($36 - 85nm$) were synthesized and deposited by drop casting over the Al-slides. The 4-Aminothiophenol molecule was used as analyte of probe at a concentration of $1.00 \times 10^{-6}M$. The size that exhibited best performance was of $55nm$, and was used in probes with Rhodamine 6G (Rh6G), Rose Bengal (RB) and Crystal Violet (CV) at low concentrations ($2.22 \times 10^{-13}, 1.00 \times 10^{-12}, 1.00 \times 10^{-10}M$ respectively). The probes with Rh6G at a concentration of $2.22 \times 10^{-13}M$ were employed to calculate the enhancement factor, giving an estimate value of $\sim 10^7$.

Further, the SERS substrate with the same characteristics was used in detection of thiram pesticide at levels close to those dictated by the FDA (7ppm). The probes showed that the designed substrate is capable of detect the pesticide alone and in a mixture with tomato pulp, even at concentrations of $10\mu M$.

El objetivo de este trabajo de tesis, es el diseño y desarrollo de un sustrato SERS eficiente, para la detección a bajas concentraciones de colorantes y pesticidas.

Nanocubos cóncavos de oro (CGNC) se sintetizaron mediante el método de reducción química. Los nanocubos se caracterizaron por espectroscopía de UV-Vis y por microscopía electrónica de barrido (SEM), para asegurar que la morfología y el tamaño fueran los deseados.

Para el depósito de los CGNC, se utilizó una base de aleación de aluminio (*Al-6063*), dado que no presenta señal Raman o de fluorescencia que pueda opacar la señal de respuesta del analito de prueba. La superficie de las láminas de aluminio se modificó, primero por tratamiento mecánico y luego se sometió a un proceso de electropulido, para después ser funcionalizados con moléculas de silano. La superficie de las láminas se caracterizó por microscopía de fuerza atómica (AFM) y por difracción de rayos X (XRD), para confirmar la presencia de pseudoboehmita en la superficie.

Con el fin de seleccionar el tamaño de nanocubo que mostraba el mayor incremento en la señal Raman, se sintetizaron soluciones de nanopartículas de diferentes tamaños $(36 - 85nm)$ y se depositaron mediante goteo sobre las láminas de *Al*. La molécula de 4-Aminotiofenol se usó como analito de prueba a una concentración de $1.00 \times 10^{-6}M$. El tamaño que mostró la mayor amplificación fue de $55nm$, el cual se utilizó en pruebas con Rodamina 6G (Rh6G), Rosa de Bengala (RB) y Cristal Violeta (CV) en bajas concentraciones ($2.22 \times 10^{-13}, 1.00 \times 10^{-12}, 1.00 \times 10^{-10}M$ respectivamente). Las pruebas con Rh6G a una concentración de $2.22 \times 10^{-13}M$ se emplearon para calcular el factor de realzamiento, dando un valor estimado de $\sim 10^7$.

El sustrato SERS con las mismas características se utilizó en la detección del pesticida llamado thiram, en niveles cercanos a los dictados por la FDA (7ppm). Las pruebas mostraron que el sustrato diseñado es capaz de detectar el pesticida solo y en una mezcla con pulpa de tomate, incluso a concentraciones de $10\mu M$.

A Margarita, Eustacio, Fanny, Fátima y Mateo.

If something burns your soul with purpose and desire, it is your duty to be reduced to ashes by it. Any other form of existence will be yet another dull book in the library of life.

Charles Bukowski

Agradecimientos

Esta trabajo de tesis, es un compendio de trabajo en el cual apoyaron y participaron muchas personas.

Quiero agradecer principalmente a mi familia, mis papás Eustacio y Margarita, por su apoyo y comprensión en este largo tiempo, por siempre estar presentes y ser mi fuerza. A mis hermanas Fanny y Fátima, por estar siempre ahí, al pie del cañón, listas para brindarme su ayuda y cariño.

A mi asesor Dr. Juan Luis Pichardo Molina, por su tiempo, enseñanzas, ayuda, comprensión y sobre todo paciencia para poder realizar este trabajo.

A mi comité de seguimiento, los doctores Oracio Barbosa, Noé Alcalá y Norberto Arzate, por sus aportes y comentarios para la mejor realización de este trabajo.

Agradezco también al Dr. Mario A. Rodríguez por su invaluable ayuda y orientación en las cuestiones químicas de este trabajo, al técnico Martín Olmos, por su ayuda en el laboratorio.

A la técnico Ing. M. Christian Albor Cortés, por su ayuda y paciencia en la obtención de las imágenes de microscopía electrónica de barrido que se presentan en este trabajo de tesis.

A los técnicos de taller Mecánico, Jesús Ramírez, Marco Troncoso y Jorge Durán; por su ayuda para el corte de piezas y resolución de problemas técnicos.

Así mismo a los técnicos de taller óptico, Alfredo Hernández Vilchez, Alejandro Blanco Soto, José Luis Flores Arias y José de la Luz Hurtado, por su gran ayuda y apoyo para el pulido del aluminio.

A todos los miembros del GPOM, que con sus comentarios ayudaron a mejorar este trabajo.

A mis compañeros de laboratorio, Pablo Cardoso, por su gran ayuda en la realización de este trabajo, Pablo M., Rigo y Fernando, sin su presencia el trabajo habria sido menos ameno.

Al Centro de Investigaciones en Óptica por brindarme la oportunidad de crecer profesional y personalmente,

A Monserrat A. López Urquieta, por su amistad y apoyo, en infinitas pláticas, consejos, comidas y jalones de orejas, muchas gracias.

A Christian Albor por su apoyo, paciencia y amistad.

A mis roomies: Yuly, Viviana, Lupita, sin ustedes, esto no habría sido lo mismo, en tanto tiempo compartido y tanto apoyo brindado, gragias por aguantar mis peculiaridades.

A las personas que me acompañaron en este camino, Cynthia, Jorge, Vanessa, Andrea, Heraclio, David, Yoshio, muchas gracias.

A CONACYT por la beca otorgada.

Contents

List of Figures

List of Tables

Chapter 1

Introduction

Pesticides are substances used to kill, control or repel plants or animals that are considered as pests by physically, chemically or biologically interfere with their metabolism or behaviour. Pesticides include herbicides, insecticides, fungicides and disinfectants [2, 3]. The last years, there has been a extensive use of agriculture chemicals in food production, making the people exposed to significant pesticide residues through the food. Based on the chemical structure and functionality, the pesticides are classified in five groups: organochlorine, organophosphate, carbamate, neonicotinoid and pyrethroid [4, 5].

The detection of pesticide levels in the environment is of huge importance to regulate and monitory its use. Since early 1970s was the interest to study pesticides, performed by immunoassay-based test and solid phase technology. In these techniques, colourant labels as enzymes, chemiluminescent and fluorescent labels are applied as detecting agents. The use of colourants require a great quantity of enzymes, and are obtained from a laborious processing, and are selective to certain pesticides, which limited the action field, besides the results were not accurate. From that, the research for a reliable, portable and accurate way of determine the presence of pesticides started [6].

Nowadays, analytical methods to measure pesticide levels on vegetables include High performance liquid chromatography (HPLC), gas chromatography- mass spectroscopy

(GC-MS), among others, but this methods have the disadvantage of being time consuming, and require of a sample pretreatment [5–8]. For it, is important to develop a fast and efficient method with excellent sensitivity.

In addition to the methods mentioned above, other technologies have emerged to offer advantages, as faster detection times, least expensive and *in situ* sampling. Surface enhanced Raman Spectroscopy (SERS) is one of this new techniques. SERS is a fusion of two techniques, nanotechnology and Raman spectroscopy, that will be described in detail in the following chapters. A SERS substrate is a combination of a roughened metallic surface deposited over a glass or silicon surface with the Raman spectroscopy. The metallic surfaces most used are gold, silver and cooper. This combination enables the intensification of the Raman signal, and thus the capacity to detect analytes. An effective SERS substrate also have to meet the criteria of homogeneity, portability, reproducibility and sensitivity.

The principal advantages of SERS (like normal Raman spectroscopy) are that there is no need of sample preparation, works with solids, liquids or gases, can work with *in-situ* and *in-vitro* biological samples, is a non-destructive and non-invasive technique, does not need vacuum to obtain the measurements, works with aqueous samples in a wide range of conditions (pressure, temperature), for remote sensing can be used optical fibers [9].

Taking advantage of its potential, several scientific articles had published the possible applications. Some of them focus on the detection of environmental pollutants in food [10], cancer diagnosis [11], biomolecules [12], among others [13, 14]. General applications of SERS also have been developed, even pesticide detection has been studied.

The pioneering work employing SERS for pesticide detection was carried out by Alak and Vo-Donh [15]. In this work, eight kind of organophosphorous pesticides were characterized using silver coated microspheres (teflon of polystyrene latex) deposited over cellulose and glass surfaces. Also a sample of pesticides contaminated soil was studied,

to prove the scope of the technique and its applications. Thereafter, a lot of publications had involving SERS substrates a way of detect pesticides.

The advantage of using SERS over other techniques to study pesticides, is that the detection of pesticides diluted in organic solvents or water do not represent any problem. The process can be as simple as deposit a drop of the pesticide over the SERS substrate and carry on a measurement.

The limit of detection (LOD) is the most studied characteristic in SERS studies for the sensitive detection of pesticides. This is defined as the sufficient analyte concentration required to produce an analytical signal that can be distinguished from analytical noise, i.e. the signal produced in the absence of analyte [16]. The reported LOD for pesticide detection depends a lot of the type of SERS substrate and the kind of pesticide used.

When are talking about pesticides, there has to be considered that the LOD (reported in ppm) is different from the MRL (maximum residue level), the highest level of a pesticide residue that is legally tolerated on food, and is based on the matrix that is present, i.e, the fruit [17]. A careful transition of units and relation between this two parameters are needed for a good performance when pesticides are under study.

The variations in sensitivity on a substrate, can be attributed to size, morphology and distribution of the NP's on the slid substrate; the last characteristic gives origin to the called *hot-spots*. These are found at the interstitial gaps between nanoparticles, and can produce an intense local field enhancement due the localized surface plasmon resonance (LSPR). The LOD of SERS substrates can sometimes reach the single molecule detection when the substrate has a hight hot spots density.

To increase the number and control the number of hot spots still represents a challenge. In some cases, the addition of an aggregation agent, increase the number of hot-spots. In this way, the repellent forces between nanoparticles, are suppressed and they can get together, making the SERS signal more intense [18]. The pre-concentration of

nanoparticles is other technique to increase these, by physical methods like filtration or centrifugation [7].

Aside from of the increase of hot spots, variations in the size and shape of the nanoparticles also can increase the strength of the local electromagnetic field and increase the affinity or contact angle with the pesticides. Morphologies like nanowires [19], nanocubes [20], nanostars [21], etc. have been synthesized to be used as SERS substrates.

The sensitivity of a SERS substrate can change due to its design, the morphology, size and material of the nanoparticles. Pesticides with functional groups as amine of thiol, as thiram or thiabendazole, can bind to Au/Ag nanoparticles in a strong way, making then good targets [22–25].

When the specificity of the NPs is not good, ligand molecules are employed to achieve it. Kubackova *et al* detected low concentrations of four organochlorine pesticides (aldrin, dieldrin, lindane and endosulfan) by means of a functionalized SERS substrate. Several types of aliphatic $(\alpha,\omega-)$dithiols were used as linkers, which induced the interparticle junctions to create hot spots and also to create an suitable enviroment to attach to the pesticide [26].

One of the limitations that keep the development of SERS technique on hold, is the reproducibility in the results with respect to the peak intensities. This variation in intensities can come from a lot of reasons, being the principal the preparation and type of SERS substrate, preparation of the sample and also the formation and control of the hot spots.

While most reports employ as basis for solid SERS substrates silica or glass, there have been works using paper [27,28], nanopaper [29], teflon [30], aluminum paper [31,32], and some other metals. Even there are commercial SERS substrates basis from different companies, amplifying the action field of the technique.

Taking advantage of the features of SERS, many research groups have advocate to the

study of pesticides, not only in the case of detection in laboratory, but also applying it to a fruit or plant of interest, in the peel as directly to the whole piece due to its fast response and low limit of detection [33–36]

Motivation: The development of a SERS substrate capable of detect low level concentrations of pesticides, by using gold metal nanoparticles. Carry out a suitable and fast method to detect low concentrations, and avoid the rejection of the product. This necessity comes from the health issues derived from the extended use and the consume of food contaminated with pesticides. Also, the implications in the economy of the farming exportation.

Objective: The main objective of this work is the fabrication and improvement of a SERS substrate by using concave gold metal nanoparticles, in order to probe its development in the detection of dyes at low concentration ($\sim 10^{-10}M$) and pesticides at levels close to those dictated by the FDA.

Chapter 2

Raman Scattering and Surface enhanced Raman spectroscopy

The Raman effect was first predicted by Adolf G. Smekal ($1895-1959$) in 1923, but first observed in 1928 by Chandrashekhara Venkata Raman ($1888-1970$) and Sir Kariamanickam Srinivasa Krishnan ($1898-1961$), fact that give Raman a Nobel prize in physics in 1930 [37].

Raman spectroscopy is an optical technique, used to provide information of the molecular structure and also of the chemical composition of a sample. Is highly specific due to the fingerprint information that gives of a sample, and to determine semi-quantitatively the amount of a substance in a sample [38, 39].

Historically, Raman spectroscopy has been described in terms of classical and quantum theory. The classical theory is based in the theory of light as a wave, and the quantum theory, taking as basis the quantized nature of vibrations.

Sample preparation is rarely an issue on Raman spectroscopy, since many materials, organic and inorganic, are suitable for analysis, and can be liquid, powder, gas or solid, and at room temperature. The problems arise when fluorescence or burning occur. Fluorescence coming from impurities, leaving to degradation in some cases [39].

Its mayor disadvantage is the weak signal due to the low scattering cross section, which limits the application in samples at low concentrations.

2.1 Raman Scattering Theory

When an electromagnetic field interacts with a molecule, light can follow one of three paths, can be adsorbed, scattered or do not interact at all. The absorption process occurs when the energy of the incident photons correspond or is really closed to the energy gaps between electronic levels, the photon can be absorbed and the molecule reaches a new excited level. [39, 40].

The scattering process is produced when a photon rises to a virtual state and immediately dissipate the energy by emitting a photon. There are two types of scattered radiation, the most intense is Rayleigh scattering, and originates when the energy of the molecular system before and after the scattering process is the same, this is, an elastic scattering.

Raman scattering is a less frequent event, since it involves only one in $10^6 - 10^8$ of the scattered photons [39]. Raman scattering is a two photon event: the incident, that is absorbed, and the second is created due to the relaxation of the excited level. This process involves electronic transitions between vibrational energy levels of the same electronic state of a molecule.

When a light wave passes near a molecule, interact and distort the cloud of electrons surrounding the nuclei, causing the polarization of the electrons and go to a higher state. At that instant, the energy present in the light wave is transferred to the molecule, resulting in a higher state of the molecule, called 'virtual state', which is not stable and the energy is released as scattered radiation.

This event occur when the light and the electrons interact and the molecule nuclei start to move at the same time. The nuclei is heavier than the electrons, causing a change

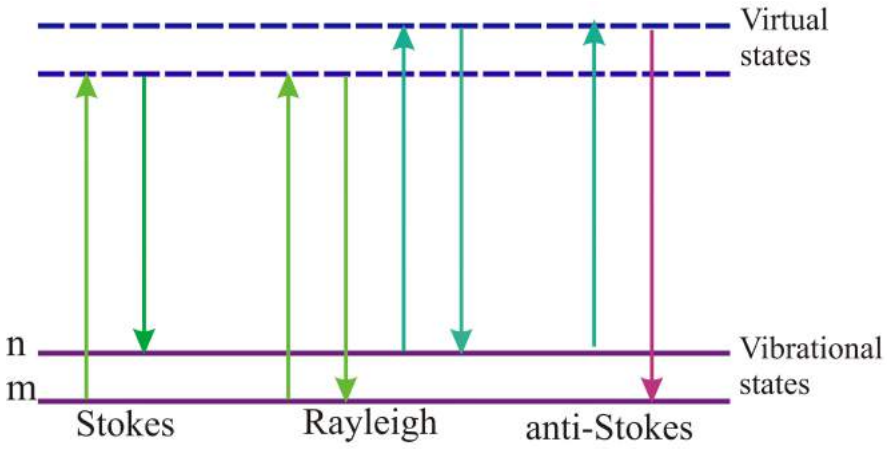

Figure 2.1: Energy level diagram of Raman scattering effect.

in the energy of the molecule either to a lower or a higher state, depending on the starting conditions of the molecule, if it was in ground state (*Stokes* scattering) or in a vibrational excited state (*anti-Stokes* scattering), this is shown in Fig. 2.1 [41].

A molecule experience three types of energy when is excited, translational, rotational and vibrational. The translational energy is described in terms of three coordinates, that determine the freedom degrees, as well as rotational energy.

The total freedom degrees of a molecule can be defined as $3N - 6$ for all molecules, except for lineal, where is $3N - 5$, since the rotation in the molecular axis does not exist [42, 43]. In the molecule, the nuclei are space and rotation fixed about their equilibrium positions, but are free to vibrate in harmonic motion along a coordinate q. When exist a vibration in the molecule, the dynamical variable will be the vibrational displacement q, which is defined as in (2.1),

$$q(t) = q_0 sin\,(\nu_{vib} t) \tag{2.1}$$

where q_0 is the normal coordinate and ν_{vib} is the frequency of the vibration molecule.

The polarizability of a molecule can be expanded in Taylor series around $q = 0$ as in

eq. (4.3a),

$$\alpha = \alpha_0 + \left(\frac{\partial \alpha}{\partial q_k}\right)_0 q_k + \left(\frac{\partial^2 \alpha}{\partial q_k^2}\right)_0 \frac{q_k^2}{2} + \dots \tag{2.2}$$

The vibrations in a molecule are defined as oscillation of the atoms in the neighbour of their equilibrium positions, and can be considered as an harmonic oscillator. The frequency of the vibrations are related with the mass of the collective vibrating atoms.

The intensities of the Raman spectrum depend of the nature of the vibration under study and instrumentation factors. Since different functional groups present different vibrational types, every molecule present a unique Raman spectrum. This molecular polarizability changes as the molecular are perturbed and change its equilibrium position [44, 45].

If the electromagnetic excitation radiation is considered as an oscillating wave, then the amplitude of the electric field $E(t)$, varies as a sine function, given by ec.(2.3),

$$E = E_0 sin\left(2\pi \nu_{laser} t\right) \tag{2.3}$$

where E_0 is the amplitude and the frequency and ν_{laser} the frequency.

This field have as effect, that the electrons in the molecule will follow their behaviour, and experience an induced dipole moment μ, causing scattered light at the oscillation frequency ν_{laser}, this is Rayleigh radiation.

The molecule suffers a distortion in its electron cloud when interacts with light, and the ease of the electrons to follow the light field, will determine the intensity of the distortion . The elasticity of the electron cloud is called *polarizability* α, when the sample is irradiated with the light of ν_{laser}, the dipole will be described as in (2.4) [40].

$$\mu = \alpha \times E = \alpha \times E_0 sin\left(2\pi\nu_{laser}t\right) \tag{2.4}$$

In Raman scattering, the molecule vibrates at ν_{vib}, giving as consequence a change in the polarizability of the electron cloud (α). This change can be represented as $\frac{\partial\alpha}{\partial q}$, i.e the polarizability of the electrons and of the induced dipole (μ) in the vibrating molecule. This is a Taylor expansion for small displacements, a function of the driving field of the photon (E_0) and the vibration. The polarizability is modulated by the vibration, and result as in (2.5), and the dipole will be described as in (2.6).

$$\alpha = \alpha_0 + \left(\frac{\partial\alpha}{\partial q}\right)_0 sin\left(2\pi\nu_{vib}t\right) \tag{2.5}$$

$$\mu = \alpha \times E = \left[\alpha_0 + \left(\frac{\partial\alpha}{\partial q}\right)_0 sin\left(2\pi\nu_{vib}t\right)\right] \times E_0 sin\left(2\pi\nu_{laser}t\right) \tag{2.6}$$

The equation (2.6) can be factorized, leaving to ec. (2.7).

$$\mu = \alpha_0 E_0 sin\left(2\pi\nu_{laser}t\right) + \frac{1}{2}\left(\frac{\partial\alpha}{\partial q}\right)_0 E_0\left[cos2\pi\left(\nu_{laser} - \nu_{vib}\right)t - cos2\pi\left(\nu_{laser} + \nu_{vib}\right)t\right] \tag{2.7}$$

The equation (2.7) tells that Raman scattering occur at frequencies above and below the excitation frequency ν_{laser} [38, 44, 46, 47].

This equations can be generalized to the case where the polarizabilities are anisotropic, and the directions of the induced dipole and the electric field are not the same. In the

absence of non linear effects, the intensity of Raman scattering increases with the 4^{th} power of the excitation frequency.

2.1.1 Molecular vibration types

The change in frequency experimented by the photons in the Raman scattering is called 'Raman shift', expressed in cm^{-1}, correspond to the wavenumber of the vibrational mode that is involved in the scattering process.

Molecular vibrations can be seen either by IR or Raman spectroscopy. Nevertheless, they offer different information, while in IR must exist a change in the dipolar moment, in Raman must exist a change in the polarizability of the molecule.

In Raman spectroscopy, the inelastic scattering contains information about the vibrational states of the sample, evidenced by a shift on the frequency of the incident light. This is, the vibrations modulate the polarizability and induce the radiation of the dipole moment at different frequencies from the incident electromagnetic radiation, this response is the one that is measured and stored by the detector.

When the vibration modes are under study, the symmetry of the molecule has to be considered as well as the change in the dipole moment.

A molecule will be infra-red inactive if the symmetry does not get altered in its internuclear separation, then the electric dipole moment remain zero during a vibration. When a molecule is Raman active, the change is its polarizability is different from zero $\left(\frac{\partial \alpha}{\partial q} \neq 0\right)$. From here, a 'selection rule' is established, the *mutual exclusion principle*, that tell that when a molecule with a center of symmetry, the vibrational modes of the molecule that are Raman active are infrared inactive, and viceversa. For example, homonuclear diatomic molecules have a symmetry center and by consequence are only Raman active [43, 48].

The Raman scattering is weak by nature, since only a small fraction of light is inelastically scattered. The Raman scattering process depends of the energy of the excitation

source, but also of the orientation of the molecule with respect of the incident field polarization. In most cases, the orientation of the molecules is random, and averaged in the measurement signal. The efficiency of a molecule to present Raman scattering is defined by a differential Raman cross section eq. (2.8).

$$\frac{d\sigma_r}{d\Omega} \tag{2.8}$$

where $d\Omega$ is an element of the solid angle, and $d\sigma_r$ is the differential Raman cross section.

The relation (2.8) characterizes the radiation profile of the scattering considering the orientation of the molecule with respect of the incident light and the observation direction with respect of the scattered light. The differential Raman cross section can be derived from:

$$\frac{dP_R}{d\Omega}(\Omega) = \frac{d\sigma_r}{d\Omega}(\Omega) S_{inc} \tag{2.9}$$

where P_R is a power of the Raman scattering process, and S_{inc} is the incident density power. The Raman cross section depends of the excitation wavelength and refractive index of the medium [49]. The differential Raman cross section characterize the magnitude of Raman scattering for a given Raman mode, and its most important characteristic [48].

As was stated before, the frequency vibrations of a diatomic molecule depend of the reduced masses m_{red} of the atoms under vibration and also of the interaction forces f between them, this can be described as:

$$\omega_{vib} = \sqrt{\frac{f}{m_{red}}} \tag{2.10}$$

This equation (2.10) shows that the lighter the atoms, the higher frequencies of vibration. The force is related to the bond, the stronger the bond, the vibration frequency will be stronger. The vibration modes can be divided in two basic types [50–52]. The Figure

2.2, describes the different vibration modes.

1. Stretching vibration ν (symmetric and asymmetric). Correspond to the contraction and elongation of the bond between two neighbouring atoms, but there are not changes in the angle of the bond (see 2.2a).

2. Bending or deformation vibration δ.

   (a) Scissoring vibration. Refers to the in plane movement of atoms, producing a change in the bonding angle. Two non bonded atoms connected to a central atom, move towards each other with a change in bond angle.

   (b) Wagging vibration ω. Implies a movement in phase and out of plane, while the rest of the molecule is in plane. Two non bonded atoms connected to a central atom, move up $(+)$ or down $(-)$ the plane.

   (c) Rocking vibration r or ρ. The atoms swing in phase back and forth in the symmetry plane of the molecule. The movement of the angles is in the same direction.

   (d) Twisting vibration t. Involves the twist of a bond along its main axis. The movement is defined by an atom moving out the plane $(+)$, while the other moves down the plane $(-)$ with respect to the main atom.

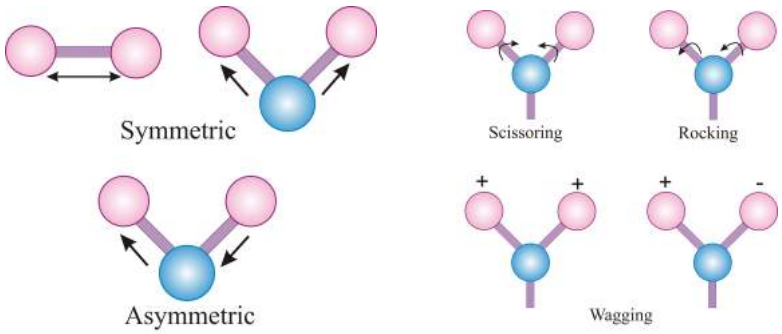

(a) (b)

Figure 2.2: Types of normal vibrational modes: **(a)** Stretching, **(b)** Bending and deformation.The arrows show the direction of deflection of the atoms; plus and minus signs point the direction of deflection of the atoms beneath and over the plane

The vibrations can be symmetrical or asymmetrical in relation to the symmetry center. The molecules are *in plane* if there are no changes in the angle between bonds and the plane defined by the remaining atoms. The vibrational modes can be classified as parallel or perpendicular depending the geometric relation between the transition moment and the symmetry axis of the mode.

The selection rule for a Raman active transition is given by eq. (2.11), and is to predict which bands will suffer a change in the polarizability during the vibration.

$$\frac{\partial \alpha}{\partial q} \neq 0 \tag{2.11}$$

Almost all molecules at room temperature are in the lowest vibrational mode with quantum number ($\nu = 0$) , and the most probable transition will be to the next level ($\nu = 1$), this transition is called 'fundamental'. By contrast, if the transition occurs to higher levels ($\nu = 2$) will result in bands called 'overtones', this kind of transition are weaker than the fundamental. Some vibrations of similar frequencies interact and get coupled, occurring an effect known as 'combination.'

The intensity of a given vibrational band in Raman spectrum, depends of the change in the polarizability by a particular vibration mode. If the vibrational mode significantly

change the polarizability will present a strong band, making it pretty discernible.

2.2 Surface enhanced Raman Spectroscopy

Surface-enhanced Raman scattering (SERS) is a spectroscopic technique in which laser spectroscopy and the optical properties of metallic nanostructures work together [53]. SERS is one of the most enigmatic and strongest phenomenons in optics and physics. The phenomenon of SERS was first observed in 1974 by Fleishman *et al* [54]. The phenomenon was interpreted later in 1977, in a work where pyridine absorbed on a rough silver electrode was studied. The idea was to increase the surface area, and as result, to increase the number of adsorbed molecules. Jean Marie and Van Duyne and Albert and Creighton separately [55], tried to give an explanation to the observed high intensities. The first two proposed an electric field enhancement mechanism, while Albert and Creighton hypothesize about an effect of resonance from the molecular states, broadened by the interaction with the metal surface [1, 44, 56–59]. Now, most authors accept both theories as valid.

The large enhancements occur with surfaces on the nanoscale $10 - 100nm$ range. The unique optical and structural properties of the metal nanostructures are highly studied and used for a variety of applications. Theoretical studies predicts strong enhancement of electromagnetic fields by the action of sharp tips and large surfaces with curves [59–63]. These surfaces include electrodes roughened by oxidation-reduction cycles, island films, colloids, and arrays of particles deposited by lithography [53].

In SERS, the surface plasmon resonance (SPR) plays a key role in the signal enhancement. SPR is probably the most important property of metallic nanostructures [56,64,65]. SERS usually has been associated with silver, gold and copper nanomaterials, but metals like rhodium and platinum also have shown a relative good SERS performance, with enhancements around 10^4. Other metals as ruthenium and aluminium remain of great

interest due their potential applications [49, 66, 67]. Although there are many ways of preparation of SERS substrates, colloidal nanoparticles might be the most popular substrate. The preparation methods will be discussed in detail in chapter 3. To understand SERS, there has to be consider the interaction between light-matter, but also the interaction between the metal nanostructures and light [1].

One of the advantages of using SERS is the capability to measure the Raman spectra from small volumes, together with the trace analytical study. There are two models to explain the enhancement of the Raman signal. One of them is the electromagnetic model, reported simultaneously in 1980 [56].

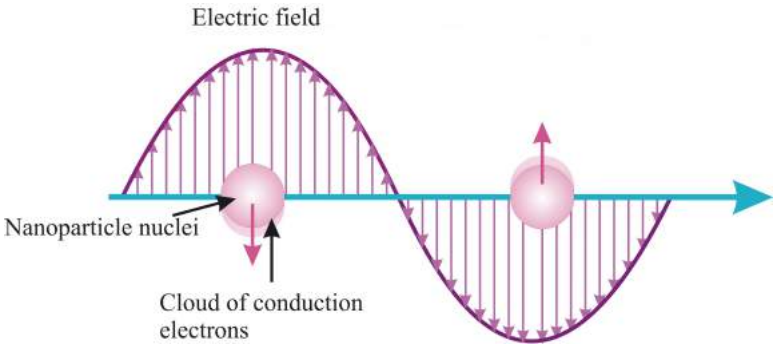

Figure 2.3: Excitation of the LSPR of a spherical nanoparticle by incident EM radiation.

2.2.1 Electromagnetic theory of SERS

The electromagnetic theory is the simplest model to interpret the enhancement on the Raman signal. This effect is based on the amplification of the electromagnetic field due to the resonance excitations of localized conduction electron oscillations at the metallic surface. The resonance produced by the excitation of localized conduction-electron oscillations in a metallic nanostructured surface is the basis of the amplification of the electromagnetic field. The collective excitation of the electron gas in a conductor, are named plasmons. When the excitation is restricted to the proximities of the surface, it is called surface plasmon (see Figure 2.3) [68]. A requirement for the excitation of surface

plasmons by light is that the surface must be roughened or with a certain curvature. The resonance in localized surface plasmons (LSPR) can be derived from the extinction spectrum.

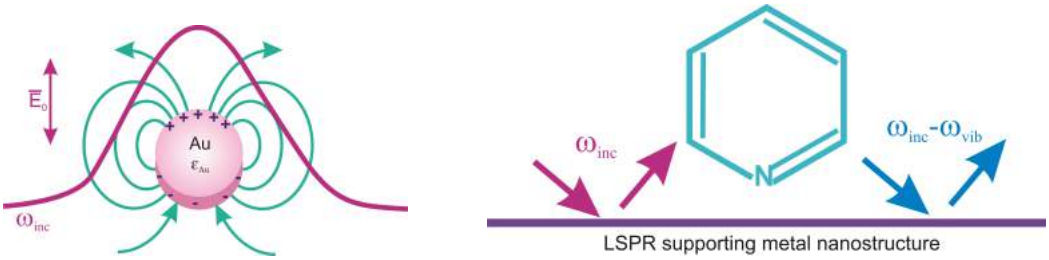

(a) (b)

Figure 2.4: SERS electromagnetic enhancement. (a)A gold nanoparticle acts as a nanoantenna by excitation of a dipolar localized surface plasmon resonance (LSPR). (b)The incoming field and outgoing field are enhanced by elastic light scattering off the LSPR supporting metal nanostructure [1]

The resonance frequency ω_{max} of plasmons depends among other parameters, of the dielectric functions of the nanometal $\varepsilon_{metal}(\omega)$ and the surrounding media $\varepsilon_m(\omega)$. The coupled state of the photon and the LSPs go with the enhanced amplitude of the electromagnetic field (EM), in the vicinity of the roughened metal surface. The adsorbed molecule at the surface then will feel a stronger E_{loc}.

The shifted Stokes frequency at $\omega_s = \omega_{inc} - \omega_{vib}$ for a particular vibration mode can excite a LSPR of the metallic structure. The local field enhancement and Raman radiation have the same physical: the coupling of the LSPR with the EM field of the metallic substrate. The total SERS intensity, then, will depend of both the incoming ω_{inc} and outgoing field $\omega_s = \omega_{inc} - \omega_{vib}$.

$$I_{SERS} = I_{inc}(\omega_{inc}) \cdot I(\omega_s) = \mid E_{inc}(\omega_{inc}) \mid^2 \mid E(\omega_s) \mid^2 \tag{2.12}$$

SERS enhancement requires that both the incident and the Stokes radiation at $\omega_s = \omega_{inc} - \omega_{vib}$ are in resonance with the LSPR peak of the metallic nanostructure. The LSPR

depends on the size and shape of nanostructures and also is modified by the closest space between nanoparticles [69].

In simple cases, I_{SERS} can be reduced to $\mid E_{inc}(\omega_{inc}) \mid^4$ factor. Moderate increase of $\frac{E_{loc}}{E_{inc}}$ drive to RS enhancement, which is termed with the SERS enhancement factor (EF). If we consider a model with a single metal sphere, which is small compared with the wavelength, and is irradiated with a laser light, will have a Raman scattering arising from the surface of the sphere. Also, the sphere is embedded in a medium with a dielectric constant ε_0, and the dielectric constant of the sphere is ε_i. The electric field of the incoming light is E_0, with a vector along the z-axis, then the electromagnetic field EFwill be described as:

$$EF_{em}(\omega_s) \cong \left|\frac{\varepsilon(\omega_{inc}) - \varepsilon_0}{\varepsilon(\omega_{inc}) + 2\varepsilon_0}\right|^2 \left|\frac{\varepsilon(\omega_s) - \varepsilon_0}{\varepsilon(\omega_s) + 2\varepsilon_0}\right|^2 \left(\frac{r}{r+d}\right)^{12} \tag{2.13}$$

where d is the distance of the molecule from the surface. The s refers to the scattered light ans inc for the incident light. The largest enhancement occur when the real part of $\varepsilon(\omega)$ is close to $-2\varepsilon_0$, and the imaginary part is small [49, 70, 71].

The SERS intensity is proportional to $\sim \frac{1}{d^{12}}$, and is rapidly decreasing with the distance d from the surface. This showed that the scattered molecule does not need to be in direct contact with the metallic surface.

There are some important points have to be recalled about SERS.

- The major contribution to SERS is the scattering coming from the metal particle rather than from the molecule , whose Raman spectrum is.
- Despite SERS intensity varies as the fourth power of the local field, the effect is a linear optical effect, that depends on the first power of I_0.
- When a molecule is adsorbed on the metal nanoparticle surface, will include contributions from the metal, an as result can be altered in its magnitude, symmetry and

resonant properties from the Raman polarizability of an isolated molecule. This is particularly important in systems where metal-molecule or molecule-to-metal charge transfer takes place, altering the resonances of the system, contributing to the chemical enhancement (described below)

2.3 Chemical theory of SERS

Also known as molecular mechanism, involves the formation of a bond between the analyte and the metal surface. This mechanism depends of the adsorption site, geometry of the bonding and the energy levels of the adsorbate molecule [57].

The bond will create surface species that include the analyte and surface metal atoms, making possible the charge transfer from the metal surface to the analyte. The formation of the surface species will increase the molecule polarizability due the interaction with the metal electrons. The enhancement is thought to come from new electronic states that arise from the formation of the bond between the analyte and the metal surface. These new states are resonant intermediates in the Raman scattering. Opposed to the radiation adsorbed or scattered through the plasmons in the surface, the radiation is absorbed by the metal, a hole is transferred into the adsorbate metal cluster, then the Raman process occurs, the excitation is transferred back to the metal and re-radiation come off the metal surface [39].

Chemical enhancement is more difficult to capture compared with the electromagnetic enhancement. The first reason is that chemical enhancement is considered to contribute to the enhancement factor in the order of $10 - 10^2$, adding the fact that almost all experimental parameters have the influence of both mechanisms, making the distinction of each effect a complicated task [1, 53, 57].

Chemical enhancement can be performed only in molecules in direct contact with the surface, so the increase will take place only in the monolayer coverage, allowing the

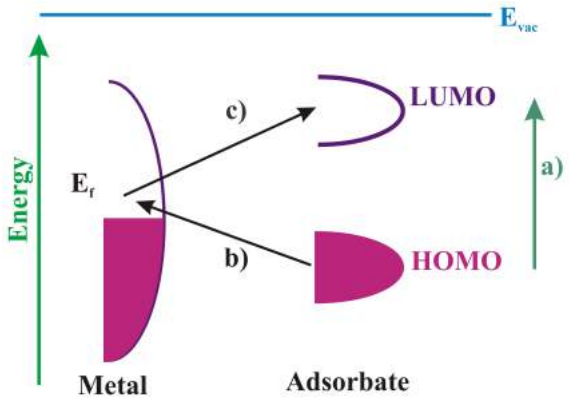

Figure 2.5: Charge-transfer mechanism of SERS. The possible interactions are shown.

formation of a charge-transfer complex between the molecule and the metallic surface.

The process of charge-transfer relate the transfer of an electron from the Fermi level of the metal to the lowest unoccupied molecular orbital (LUMO) of the molecule. The electronic states of the molecule adsorbed are shifted and broadened by means their interaction with the metallic surface, or new electronic states arising from the chemisorption help as a link in the resonant intermediate states (Fig. 2.5) . It is common that the HOMO and the LUMO of the molecule are energetically symmetric with respect to the Fermi level of the metal [57].

2.4 Calculation of Enhancement factor

The magnitude of the signal enhancement in SERS has been an important issue for many research since the discovery of the effect. The main conflict to understand the effect was based in the calculation of the magnitude of the effect, as well as estimating the number of molecules that contribute to the signal.

In the first interpretation of SERS, was postulated that the increase in signal was a result of an apparent increase in the cross section of the molecules, resulting in the concept of enhancing factor (EF). The EF is one of the most important numbers in order

to characterize SERS, specially for practical applications where the concern is to know the magnitude of the EF achieved. EF's in the order or $10^7 - 10^8$ are good enough for detection in SERS, but few works have reported EF's in the order of $\sim 10^{10}$, also in the order of 10^{12} in the best possible experimental conditions [72, 73].

The EF depends a lot of the exact SERS conditions: the substrate, the analyte, the excitation wavelength, etc. The discrepancy on the reported EFs is result of the variability in the definition of EF and the way that is calculated. The diversity of situations that can originate in SERS, as single molecules, multiple molecules, the experimental limitations, the averages over time, orientations of the probe on the surface, spatial distribution, leads to making a simple and general definition for the EF a difficult task, therefore, there are three main definitions of EF.

1. **Single Molecule EF**. This is the enhancement felt by a specific molecule in an exact point, depends of the Raman magnitude of the probe and the orientation on the SERS substrate and with respect with the local field at that given point. Due to this conditions this definition is more appropriate to theoretical estimations, instead of experimental measurements. This is defined as:

$$SMEF = \frac{I^{SM}_{SERS}}{\langle I^{SM}_{RM} \rangle} \tag{2.14}$$

where I^{SM}_{SERS} is the SERS intensity of the single molecule, and $\langle I^{SM}_{RM} \rangle$ is the average Raman intensity per molecule.

The eq. 2.14 can be defined with the orientation averaged [SMEF] at a position

$$OASMEF = [SMEF] = \frac{[I^{SM}_{SERS}]}{\langle I^{SM}_{RM} \rangle} \tag{2.15}$$

2. **The SERS substrate point of view.** Can be used to compare the average SERS enhancements over several substrates. The most of the studies have focussed on this

aspect, as defined in eq. 2.16.

$$EF = \frac{I_{SERS}/N_{Surf}}{I_{RS}/N_{Vol}} \tag{2.16}$$

where $N_{Vol} = c_{rs}V$ is the average number of molecules in the scattering volume V for the Raman measurements, and N_{Surf} is the average number of adsorbed molecules in the scattering volume for the SERS measurements. This definition presents some problems, and there is an alternative equation to work with.

$$SSEF = \frac{1}{A_M}\int_{A_M} OASMEF(r)dS \tag{2.17}$$

where A_M is the surface area of the metallic substrate. The last equation can be rewritten as

$$SSEF = \{OASMEF\} = \{[SMEF]\} \tag{2.18}$$

where the term between $\{[SMEF]\}$ is the spatial and all oriented averaged SMEF. The SSEF can be rewritten in terms of experimentally measured data as in eq. 2.19

$$SSEF = \frac{\frac{I_{SERS}}{\mu_M \mu_S A_M}}{\frac{I_{RS}}{C_{RS}H_{eff}}} \tag{2.19}$$

where C_{RS} is the concentration of the solution used for the non-SERS measurement, H_{eff} is the effective height of the scattering volume, μ_M is the surface density of the individual nanostructures, and μ_S is the surface density of molecules on the metal.

3. **The Analytical Chemistry Point of View.** The described before, have emphasized the characteristics of the substrate, and are not so easy to relate with the experimental measurements. In a lot of applications, the goal is to find the lowest detectable signal, in comparison with the Raman simple under the same conditions.

To solve this problem, there is a third definition of the SERS-EF. A solution with concentration C_{RS} produces a Raman signal I_{RS} under non SERS conditions. For the same exact experimental conditions, the same analyte on a SERS substrate with possible different concentration C_{SERS} gives a signal I_{SERS}, then the EF will be calculated as:

$$AEF = \frac{I_{SERS}/C_{SERS}}{I_{RS}/C_{RS}} \tag{2.20}$$

The AEF however, ignores the fact that SERS is a surface spectroscopy, for it, is not a good characterization for SERS substrate, and can not be used to compare the performance of different substrates.

2.5 Characteristics of SERS substrates

SERS has been identify as a powerful molecular spectroscopic technique, which permits a highly sensitive detection and non destructive characterization of molecules and biomolecules [44, 74]. One of the uses of the SERS technique is application as sensor: for the detection of molecules, biomolecules, chemical agents and warfare [44, 62, 68, 75].

There are a huge variety of methods to fabricate SERS substrates, and for practical purposes divided in two main groups:

1. **Top down approaches**. In this fabrication method, a metal layer is deposited over a surface, either roughened or nanoscale arranged. This method allows to have a symmetry, gap size control and well-controlled nanoscale patterns. Lithography, nanosphere lithography, nanoidentation or 'film over spheres' plataforms are promising techniques for fabricating SERS substrates [33, 76–78].

2. **Bottom up approaches.** This approach is realised by assembling small nanoparticles into ordered nanostructures array. Through inexpensive techniques can give

small gap sizes, but is hard to obtain highly uniform structures at a large area. Advances in this technique have allowed assemblies of metal noble nanospheres [79], nanorods [80], nanostars [21], nanocubes [81] and other morphologies [33, 77, 82].

Despite the fabrication method, an effective SERS substrate must fulfil certain requirements [83].

- The metallic nanoparticles should be placed periodically.
- The fabrication must be sample to sample reproducible.
- The signal enhancement must be uniform point to point.
- Long term stability.
- Insensitive to environmental conditions.
- Applicability to different analytes.
- Low cost.

Although not all SERS substrates fulfil the requirements, there are a lot of research looking for its improvement and higher enhancements.

In this thesis, the enhancement factor was calculated using the SERS substrate point of view criteria, since it considers the density of nanoparticles and the number of molecules that contribute to the SERS and Raman signal, not only the measured intensities.

Chapter 3

Nanoparticles synthesis and Characterization techniques

Gold has been extracted and used for humanity since ancient times. For example, colloidal gold was used to make ruby glass and for colouring ceramics, one of the most famous examples is the Lycurgus cup, manufactured by the romans in the fourth century [64,84]. The beginning of fabrication of nanoparticles in a scientific way was first made in 1857 by Michel Faraday [68, 75, 84]. He observed the formation of a red solution product of the reduction of choloroaureate ($NaAuCl_4$) by using phosphorous in CS_2 in a two-phase system [85]. He found that colloidal gold exhibited different optical and electrical properties [86, 87].

A nanomaterial, defined by the European Comission (EC) is a natural, incidental or manufactured material which contain particles as conglomerate, aggregate or in a unbound state, where at least 50% of them have dimensions in the range of $1 - 100nm$, or either one of its dimensions are in the range, can be considered as nanoparticles [88, 89].

The methods of preparation of nanomaterials have been improved in the last years, due to the big interest on its properties, and the potential applications of them in many fields of science [12, 90].

For the manufacture of nanoparticles there is a wide variety of methods. In general, metal nanoparticles are synthesised by several methods, that can be divided in two categories: physical and chemical routes [91].

3.1 Physical methods

The physical processing implies physical power and a phase reaction, either gas or liquid. The nanoparticles synthesized by physical methods, are fabricated starting from a bulk material and are processed of different ways depending of the material and the desired nanoparticle properties and size [91]. Because this method start from bulk material, are called *top-down* approaches. Some of the methods encompassed in this category are:

1. High-energy ball milling
2. Wire explosion
3. Laser ablation
4. Ion sputtering

Even through this methods can produce big quantities of material, the control of the particle size is not so easy to achieve; that is why this method is used mainly for soft metals.

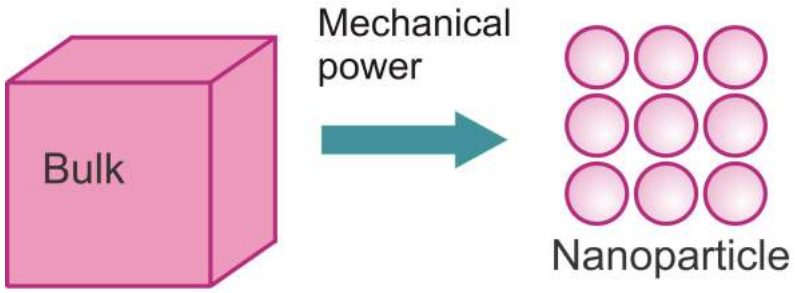

Figure 3.1: Fabrication scheme of physical processing

3.1.1 High-energy ball milling

The mechanism of nanocrystallization by high-energy ball milling was first proposed by H.J. Fecht in 1983. During high-energy milling, the powder particles are repeatedly flattened, cold welded, fractured and re-welded. Whenever the ball collide, some amount of powder is trapped between them. The impact causes plastic deformation, causing work hardening and fracture. The formed surfaces weld together, and at this point, the composite particles have a characteristic layered structure, consisting of combinations of the starting constituents. As deformation continues, the particles become work hardened and fracture. When fracture predominates over cold welding, the particle is refined. The minimum size achievable by high-energy ball milling ($\sim 10nm$) has been related to several physical properties of elemental metals. The majority of nanocrystalline metals have been synthesized in order to understand the mechanism of nanocrystallization [92].

3.1.2 Wire explosion.

A fine wire of metal is exploded by applying a high voltage. The gas of the generated atoms by the explosion is allowed to condense in the chamber to yield nanoparticles. This technique can lead to the formation of metallic nanoparticles, and also to a variety of oxides, nitrides, etc by using different environments in the chamber [92].

3.1.3 Laser ablation.

Laser ablation of solids in liquids has acquired more interest in production of nanoparticles. The basis of this method is focusing a laser beam through a transparent liquid to a metal target surface. The interaction of the laser irradiation with absorbing media causes ablation to the latter and spattering of their material in air. Nanoparticles form due to collision of molecules with each other during adiabatic expansion and recombination of the flame gas in the rarefield gas. The function of size distribution of the particles can

vary during the irradiation due to absorption at the wavelength of irradiation. One of the advantages of this method is that the synthesis can be realized in a solution without the needing of chemical reagents, obtaining high purity grade products [93].

3.1.4 Ion sputtering.

Ion sputtering process consist of ions or atoms of a suitable substance, as Argon or Krypton, accelerated to high energies, and directed to a surface, where atoms and clusters are ejected. By means of this technique, high melting point materials as ceramics and refractory metals which are difficult to convert to nanomaterials by other techniques, are able to be deposited. Ion sputtering can result in better stoichiometric control of the film, but have the disadvantage of being prone to contamination due to the lower purity of the sputtering target materials [92, 94].

3.2 Chemical processing

Chemical processing covers a lot of build-up methods, due to permits the manipulation at a molecular and even atomic level and also allows more homogeneity of the particles. This synthesis method is based on the chemical reduction (by a reducing agent)of metal ions to metal atoms, followed by the formation of clusters and metal nanoparticles [61].

This methods are also called *bottom-up* approaches [12, 85, 91]

There are several kinds of reductants, and depending of the one used, is the name to apply to the synthesis.

1. Chemical reduction
2. Micelle and microemulsion synthesis
3. Photochemical synthesis

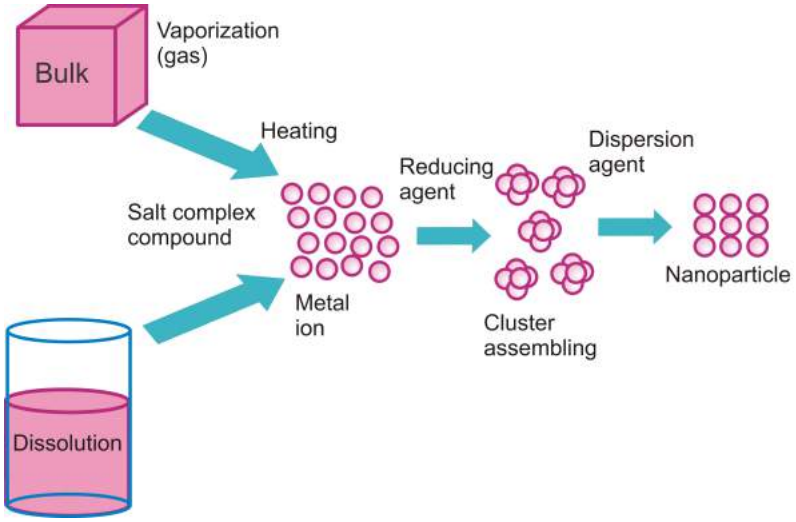

Figure 3.2: Fabrication scheme of chemical processing

4. Electrochemical synthesis

5. Biological methods.

To prevent the aggregation of the nanoparticles, some stabilizers are added to the synthesis, and sometimes the reductant is a the same time the stabilizer.

The nanoparticle usually is formed by two items, a core that can be metallic, ceramic or polymeric; and a thin shell that also can be organic, polymeric, ceramic or metallic. In general, this two entities present chemical affinity with each other, and gives stability to the system, and also, depending of the molecule, can made the nanoparticle hidrophobic or hydrophilic.

3.2.1 Chemical reduction

The reduction of metal atoms from metal ions can lead to the formation of nanoparticles by aggregation. Usually, to form a metallic nanoparticle, a metal salt is used as a initial material, since it contain ions and by means of a reductant, are converted to atoms, and later aggregated to form the nanoparticle.

The reductant to be used, depends of the way the synthesis want to be carry out, strong or middle, if only want to take place in the surface of gold [68].

Seed mediated grow method

The seed mediated grow method is a modified version of the Zsigmondy's nuclear method [85], and is one of the most used methods to synthesize anysotropic nanoparticles. Generally, this reactions are carried and the product owns colloidal characteristics [95], and presents a more wide offer of architectures than one step reduction [86]. This method consists of two steps:

1. This step also known as nucleation, involves the seed preparation. The seeds are produced by the reduction of a metal salt in an environment like water or gas and with an stabilize agent. Usually, strong reductant are used, such as sodium borohydride ($NaBH_4$) or lithium aluminum hydride ($LiAlH_4$).

2. In the second step, a growth solution is prepared, it contains an excess of metal ions, the surfactant/stabilize agent and a mild reductant. The prepared seeds are added to this solution, allowing a regrowth of the seeds. The adding of small seed particles determine the size of the resulting nanoparticle, since influence the production of monodisperse size particles. If the seeds have well defined shape, can influence the shape of the resulting nanocrystal after the final growth step [96].

The shape control at crystallographic level, can be achieved by employing capping agents that adsorb to specific crystal planes, and through this interaction make one specific facet stabilize; the growth will be limited on the crystal plane where binding is strong, while the ones that this interaction is weak, will have a promoted growth [91, 96, 97].

There are few molecules that present this selective binding between faces, however empirical experiments have shown a variety of molecules that facilitate shape control, as surfactants, polymers and biomolecules that help to avoid the clustering.

The surfactants are effective to prevent oxidation, besides prevent clustering and agglomeration of the nanoparticles, also allows mass production and high metal nanoparticles concentration [91]. Since some surfactants poses a hydrophobic tail and an hydrophilic group, they are easy to assemble into micelles (Fig 3.3) in water, depending of its concentration and co-surfactants present in the solution. In conclusion, the size and morphology of a nanoparticle depend of the type of solvent, surfactant, and reducing agent, as well as by temperature.

3.2.2 Electrochemical synthesis

This process was first proposed by Reetz and Helbig in 1994. They demonstrated that by adjusting the current density, high selective nanoparticles can be synthesized by electrochemical reduction. Structures like cubes, rods, plates, etc can be obtained [85]. The preparation of metal nanoparticles by electrochemical methods is performed by means of electrocrystalization of metals from the salt solutions or melted salts during the electrolysis. The process is carried out in electrolytic bath containing a reducing agent in solution with the ion to be reduced. Under constant current, the reducing agent is oxidized on anode and the metal ion is reduced on the cathode. The metal deposited on the cathode may have a various structure.

The morphology of the deposits depend of a lot of factors, as the nature of the solvent, the metal salt composition, the reducing agent, concentration, etc. The technique allows the preparation of nearly thirty different nanosized metals [89].

3.2.3 Synthesis in reverse micelles

The study of the creation and properties of reverse micelles began in the late 1970's. The synthesis in reverse micelles allows the preparation of stable metal nanoparticles in an organic solvent, and control the size particle by changing the hydration extent, that

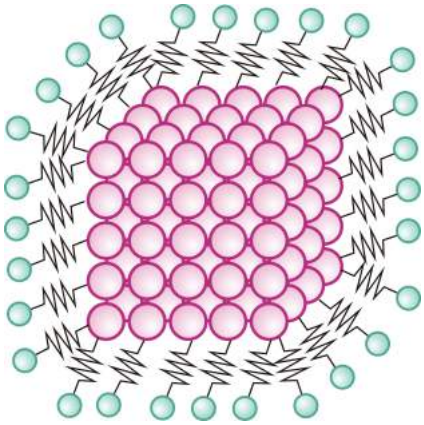

Figure 3.3: Image of a micelle particle.

defines the diameter of the water core, where the metal ions are reduced to form the nanoparticles. Reverse micelles represent a ternary system with a general composition consisting of water, a surface active substance (SAS) i.e a surfactant and a non-polar solvent (nPS) $H_2O/SAS/nPS$. This is, a reverse micellar system is a water solution in the non-polar solvent, where water is enclosed into the shells, consisting of surfactant molecules (polar heads inside, non-polar tails outside).

Reduction of the metal ions and the formation of nanoparticles take place inside the micelle. To obtain micellar solutions, cationic, anionic, and non-ionic surfactants are employed. The choice of surfactant-solvent combination is determined by the possibility to fabricate reverse micelles. The geometry of the surfactant determines the ability to form invert or direct micelles. The size is determined by the concentration ratio of the reagents and on the metal and surfactant ion concentrations. The synthesis in reverse micelles allows to obtain nanoparticles of various metals that are often more resistant to aggregation and air oxidation than the same molecules in water.

3.2.4 Photochemical synthesis.

Metal nanoparticles can be synthesized in solution by exposing the metal-ions solutions to UV and visible radiation or γ-radiolysis [12, 98]. In photochemical radiation two forms of illumination are used, continuous or pulsed. An advantage of this method is the possibility of nanoparticle synthesis in various media, as solid or polymeric. Further the desired product is obtained chemically pure, without metallic impurities, which is a common inconvenience in chemical reduction.

To create the nanoparticle in liquid media, molecular or micellar solutions with reducible compounds are used. When an aqueous solution is exposed to light, hydrated electrons, hydrogen atoms and hydroxyl radicals are formed.

To increase the nanoparticle lifetime in water or water-alcoholic solutions, several stabilizers are added, as citrates, polymers like polyvinyl alcohol(PVA), polyvinyl pyrrolidone(PVP), phenylpropanolamine (PAA), etc. Irradiation time plays an important role in this synthesis, the yield of the nanoparticles may increase with time as consequence of the of reducing particles in solution, but also influences the size, causing an increase or decrease in size [12].

3.2.5 Biological methods.

This synthesis method use natural biological substances extracted from plants or animals, aqueous extracts from living organisms or from living organisms. The advantages of this method are the soft synthesis conditions and the lower use of poisonous products in the nanoparticle solution, due to the use of reductants. For this reason, this 'biological' reduction is very promising for its application in medicine and biology, where is important an environment the less toxic possible. These methods appear in the literature with different names: *green synthesis, biosynthesis, biochemical synthesis, biological reduction.* The most numerous group is comprised by the nanoparticles synthesized with the use of

plant extracts, where different parts of the plant are employed, as the leaves, stems and roots; also extracts from seeds and fruits are applied. The rate of nanoparticle formation varies from minutes to days, and the stability in solution in air can last from weeks to months.

3.3 Characterization techniques.

The multidisciplinary characteristic of nanoscience, allows the use of multiple instruments to characterize them. There are specific techniques, that depending the properties under study (size, shape, crystallinity, etc.) is the one to be selected for the study.

To study size and shape transmission electron microscopy (TEM) and scanning electron microscopy (SEM) techniques are the most useful techniques, sometimes used indistinctly, but have the advantages by using each one of them. Electron microscopy works with accelerated electrons bombarding the sample, the scattered or transmitted electrons are detected.

SEM is one of the most popular and widely used techniques for the nanomaterials characterization. Produce accurate images with resolution of a few nanometres and magnifications up to $1,000,000x$. The acquired image is made up from the electrons that are reflected (backscattered electrons, BSE) or from the emitted ones (secondary electrons, SE) from the surface of the sample. The sample is analyzed by scanning the surface in a raster scan pattern with an electron beam, where the electrons acceleration can go from $1keV$ to $50KeV$. Secondary electrons coming from the sample surface are those which determine the surface characteristics of the sample. In addition, SEM can also give information on chemistry, crystal orientation and internal stress distribution of the sample [88, 92, 95].

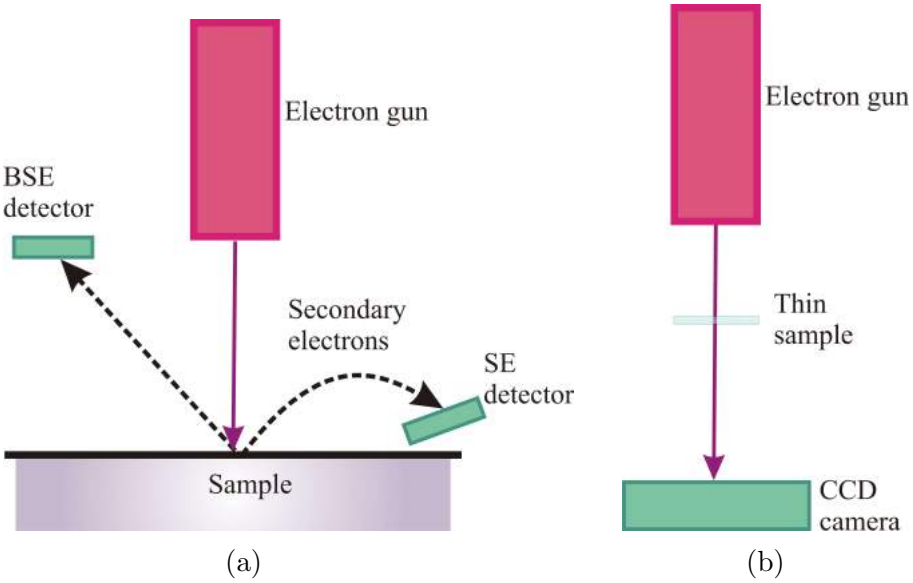

Figure 3.4: SEM and TEM schemes

TEM is capable of produce magnified images of thin specimens and additionally can give information about the crystalline properties and lattice structure of the material. In TEM, the electrons travel through a very thin sample ($\leq 200nm$), and are collected by a detector at the rear side. When the electron beam passes through the specimen, the interaction with the electrons present in the specimen generates a variety of radiation, which gives a lot of information about the sample. However, lack of contrast or overlap of particles, frequently complicate the analysis of images, since the particle boundaries can not always be determined with precision [94].

Both of them can be used in association with electron diffraction analysis and energy-dispersive X-Ray spectroscopy (EDS) and get to know the chemical composition [99].

The optical properties are measured with a wide variety of techniques, such as absorption, photoluminiscence (PL) and PL excitation (PLE) spectroscopy, and give information about the energy level structure of the samples, the presence of a dopant or defects in the material [61]. The aforesaid techniques employ electromagnetic radiation focused over the sample, and the spectra is obtained due to the interaction of light and matter.

The light transmitted by a solution, decreases as the concentration of the solution increases,(*i.e.*, the chromophore in a solution increases)and the instrument measure this change, making a comparison between the transmitted light in a solution containing a chromophore and also without it. [100].

X-ray diffraction (XRD) is used to study the crystalline phases of solids and its structural characteristics. Is a non-destructive technique and does not require detailed sample preparation. The measurement is carried out by focusing a beam of X-rays ($0.07 \leq \lambda \leq 0.2nm$) over the sample, which is diffracted by the crystalline sample, following Bragg's law ((3.1)).

$$\lambda = 2d\sin(\theta) \tag{3.1}$$

where d is the interplanar distance and λ is the wavelength of the X-rays. The intensity of the diffracted beam is measured as function of the diffraction angle (2θ) an of the sample orientation. A shift in the X-ray peak positions indicates a change in the $d-$spacing, caused by a change in the lattice constants.

Due to the lower energy of the used X-ray beam, the XRD intensities are low, specially in the case of low atomic number materials, making the detection of phases of small volumes a hard task [92].

Atomic force spectroscopy (AFM) is a high resolution image probe microscopy. Is based on the physical scanning of the samples. The principle of this technique involve a piezoelectric scanner which moves across the sample surface. The tip is mounted on a cantilever of constant force. When the tip is in contact with the sample surface, experiences a very small force ($\sim nN$) as a result of the interaction with the atoms in the surface. The tip scans across the surface, and experience attractive and repulsive forces, associated with the Van der Waals forces, and the movement of the tip will be registered by deflection of a cantilever. AFM offer several advantages over electron microscope, since it provides a true three dimensional surface profile, and can work in ambient or even liquid

environmental solutions [94].

Ultraviolet-visible (UV-vis) spectroscopy is widely used to quantitatively characterize organic and inorganic nanosized molecules. The technique consist in irradiate a sample with ultraviolet and visible electromagnetic radiation, and the absorbed light is analysed through the resultant spectra. The energies associated with radiation in range UV-vis are good enough to excite molecular electrons to higher energy orbitals. Since is a technique which operate with the principle of absorption of photons, is an ideal technique to determine the electronic properties of a material. In the spectrum of absorption of the samples, the peak's width depends strongly of the chemical composition and of the particle size. UV-vis spectroscopy not only is used for characterization, also is used for sensing applications, and has the advantage that samples can be either liquid, solid or in gaseous form, organic or inorganic nanomaterials [101].

In this thesis work, SEM was used to characterize the morphology and size of the nanoparticles, while AFM and DRX was used to characterize the base of the SERS substrate, while UV-vis spectroscopy was used to determine the resonance plasmon region.

The SEM system used to acquire images was a JEOL JSM-7800F, and the used magnifications were $30,000, 50,000$ and $100,000x$. The diffractometer was a D2Phaser Bruker, the data were obtained in a range of $10^o < 2\theta < 80^o$ in steps of 0.02 at room temperature. The UV-Vis spectra were obtained with a Stellar-Net spectrophotometer with lamps of tungsten and deuterium.

Chapter 4

Experimental methods

4.1 Concave gold nanocubes synthesis

4.1.1 Chemical materials

Chemicals and reagents: Hexadecyl-trimethylammonium chloride (CTAC,$\geq$ 98.0%), hydrogen tetrachloroaurate gold III ($HAuCl_4$, 99.99%), sodium borohyride ($NaBH_4$, 99.99%), silver nitrate ($AgNO_3$, 99.0%), Hydrochloric acid (HCl, 38.0%), 3-aminopropyltriethoxysilane ($APTS$, 99%) and 3-mercaptopropyl trimethoxysilane (MPTS) were acquired from *Sigma-Aldrich*, while L-ascorbic acid ($>$ 99%) was acquired from *Alfa Aesar*; ultra pure water from a Milli-Q system (Milli-pore, America, resistivity ($> 18M\Omega cm$) was used throughout the experiments.

4.1.2 Synthesis

The synthesis carried out for this work, is a modified version of the work presented by Zhang *et.al.* [102]. This synthesis is a two step process, as described in subsection 3.2.1.

Seed solution was prepared by sequentially adding $5mL$ of CTAC solution ($0.1M$), $250\mu L$ of $HAuCl_4$ at $10mM$ and $380\mu L$ of ice-cold $NaBH_4$ at $10mM$ under rapid stirring

at room temperature. After sodium borohydride is added, the solution must change from yellow to a brownish color. The solution is kept undisturbed for about two hours before being used. After this, the seed solution's UV-vis absorption spectra was obtained and the absorbance was set at $0.4 O.D(\lambda = 520nm)$ by adding CTAC solution ($0.1M$).

The growth solution was prepared, by mixing under rapid stirring in the following order

- $10mL$ of CTAC at $0.1M$
- $500\mu L$ of $HAuCl_4$ at $10mM$
- $500\mu L$ of $AgNO_3$ at $10mM$
- $200\mu L$ HCl at $1M$
- $120\mu L$ of Ascorbic acid at $10mM$

To tune the size of the nanoparticles, the volume of seeds that are added to the growth solution change. This volume depends of the desired size of the nanoparticle. The solutions are left to settle for about 12 hours, and the absorption spectra is obtained.

Then, the NPs are washed an concentrated by centrifugation. The velocity was selected for each case, depending the size of the nanoparticles. By this way, the surfactant (CTAC) and the possible remains of the reaction are removed. The centrifugation velocities were around: $3500 - 1000rpm$, depending of the size of the NPs, the highest velocity is for the smallest size, and viceversa. The nanoparticles get down and form a pellet, while the surfactant remains in the solvent (supernatant). The centrifugation is effective when the most of the NPs settle and the solution gets clear. Then, the supernatant is removed and replaced by water, and the NPs are redispersed in a sonication bath, and they are put again under centrifugation.

This process is repeated at least three times, in order to get clean NPs. In the last wash, just enough water was added to redisperse the NPs, without causing the aggregation and provoke their lost.

4.2 Substrate preparation

SERS substrates traditionally have been made employing a glass or silicon as basis to deposit the nanoparticles [103]. Silicon presents a strong peak at $520cm^{-1}$ but does not present fluorescence signal, making it suitable for Raman analysis, but has the disadvantage of a high cost, while common glass is a cheap material, but present high fluorescence signal, that can overlap the Raman signal of the sample.

Aluminum and copper foil had been used as substrate in a lot of works [31,85,103–105], but have the disadvantage of being too flexible, making the surface do not be uniform.

Aluminum is the most common metal element found in earth, one of its crystalline forms is the pseudoboehmite, used mainly as catalyst [106]. There are many chemical reactions to synthesize pseudoboehmite, most of them include heat treatment, resulting in a powder [107, 108].

In this work, easily available aluminum alloy 6063 (*Al-6063*) slides were employed as a basis for a SERS substrate, resulting in a low-cost functionalized substrate. *Al-6063* is a very common and cheap alloy used widely in machine shops. The aluminum alloy 6063 slides ($43mm \times 20mm \times 1.5mm$) were attached using beeswax onto the surface of the lower stainless steel disk of the polishing system. Then, aluminum oxide solution ($25\mu m$) was used as abrasive; the solution is applied constantly to the slides until the planarity of Al surface was in the order of $1\mu m$. At this time, the disk was removed of the machine to wash the slides with soap under continuous flow of water, and then sandpaper ($2500grit$) was used to remove the residual aluminum oxide from the slides and washed with soap and rinsed in water one more time. Next, the slides were dried with compressed clean air.

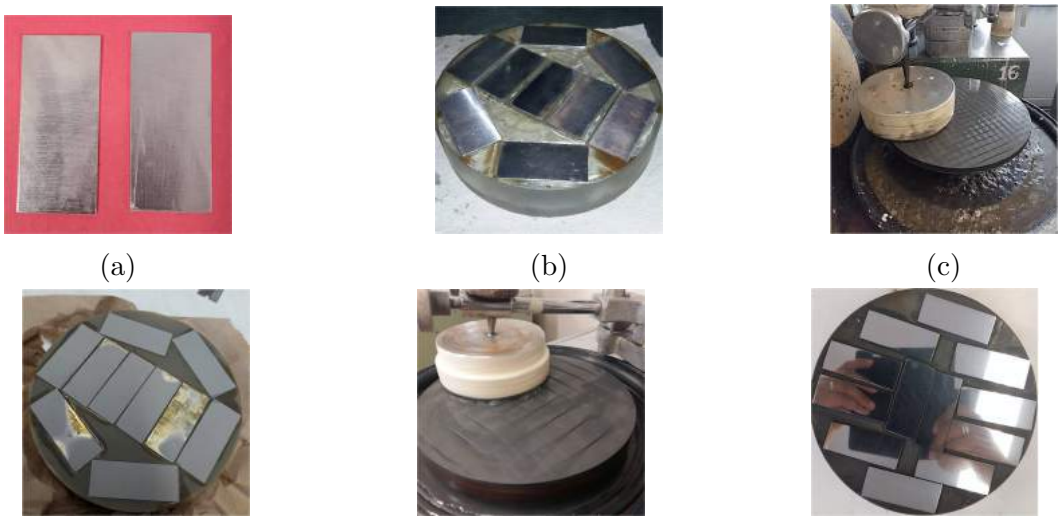

Figure 4.1: Mechanical polishing process of aluminum slides. **(a)** Aluminum slides before mechanical polishing. **(b)**Al-slides glued to a base with beeswax. **(c)**The slides are polished with alumina oxide. **(d)**The slides are polished untill all the surfaces are touched. **(e)**The slides are polished with metal polish and cotton fabric. **(f)**Slides with mirror finishing.

In a second step, the Al slides were polished by using commercial $Brasso^{TM}$ as an abrasive. The process was followed until the surface shown a mirror finishing. The same process was carried out in both surfaces of the slides. Once the mechanical polishing is done, the slides were removed from the disk and washed to eliminate the excess of $Brasso^{TM}$. The whole process is illustrated in Figure 4.1.

4.3 Electrochemical polishing

After mechanical polishing, the *Al-6063* slides were electrochemical polished in the following way: first the slides were ultrasonic cleaned in acetone three times for $10min$ to eliminate any left residues of grease and dried with compressed clean air. A solution of methanol and perchloric acid ($HClO_4, 70\%$), was prepared in a concentration $(4:1)$ [109–111] under continuous magnetic stirring and maintained in ice cold bath.

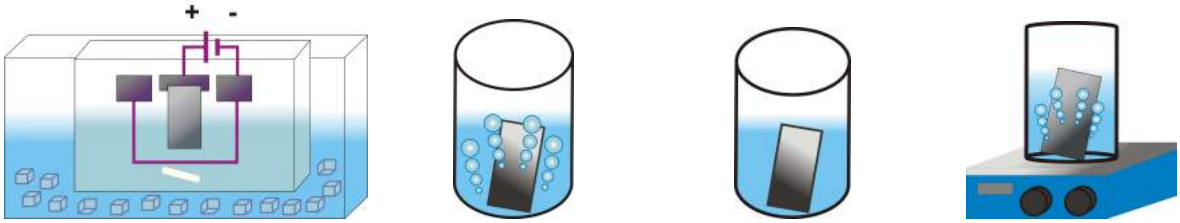

(a) (b) (c) (d)

Figure 4.2: Process of electrochemical polish. **(a)** $HClO_4$ + Etanol (1 : 4). **(b)** $NaOH, (1.5M)$. **(c)** $HNO_3, (1.4M)$. **(d)** Boiling Water for $2min$.

The *Al-6063* slide is connected to the positive terminal of the direct current power supply, while two stainless steel electrodes are connected as cathodes. While the Al slide is immersed in the ethanol-perchloric acid solution at $10C$, $2.5A$ and $25V$ for $30s$ are applied, as is shown in Figure 4.2a.

The electropolished *Al-6063* slides then were thoroughly rinsed with deionized water, dried with compressed clean air, and soaked for one minute in a solution of $NaOH, (1.5M)$ to eliminate the residual oxides; afterwards, the smut layer caused by the alkaline etching was removed by immersion in a nitric acid solution ($HNO_3, 1.4M$) for $30s$, and once again, the slides were thoroughly rinsed using deionized water and dried with compressed clean air.

(a) (b) (c)

Figure 4.3: Aluminum slides. **(a)** Before any tratement. **(b)** After mechanical polish. **(c)** After electrochemical polish.

Finally, the Al slides were hydrothermally treated by placing them into boiling water for $2min$. This last treatment allows the formation of pseudoboehmite ($\gamma - AlO(OH)$ [110], and in turn, the hydroxyl groups of ($\gamma - AlO(OH)$ allow the modification of the surface of the solid substrate through silanization. In Figure 4.3, images of the slides are

shown, after any treatment and after the polish.

4.4 Substrate funcionalization

Lastly, the substrates were silanized using APTS and MPTS in a methanol solution (2%, $20mM$), for $15h$. The slides were first cleaned with ethanol and then with deionized water in an ultrasound bath two times for 10 min each, and blow dried using compressed clean air, after which they were placed into an oven at $110C$ for $30min$ to eliminate the residual unbound APTS or MPTS from the Al surface. The slides are stored under dry conditions, to avoid the oxidation of the polished surface.

Chapter 5

Results and Discussion

The *Al-6063*, as well as the NPs, were characterized by different techniques. To confirm the presence of the pseudoboehmite, in the case of the Al-substrates. For the NPs, the characterization of morphology, size and deposition are important issues concerning SERS. The SEM image that show the pseudoboehmite present in the *Al-6063* substrate is shown in Figure 5.3. While the DRX analysis is shown in Figure 5.1.

5.1 Aluminium Substrate characterization

The formation of a pseudoboehmite layer over the *Al-6063* was confirmed by X-ray diffraction (XRD, *D2 Phaser Bruker*, with a Bragg-Brentano geometry and $Cu - \kappa\alpha$ radiation ($\lambda = 1.5418\mathring{A}$), using the following scan: step size $= 0.02°, t = 5s, 10° \leq 2\theta \leq 80°$), see figure 5.1. The reflections of the pseudoboehmite correspond to $(020), (120), (031), (200), (151), (002)$ and (251) planes, in accordance with the reference standard $21 - 1307$ *JCPDS*. Since the peaks are broad, can be inferred that the material present small crystallite size and also present poor crystalline properties [112].

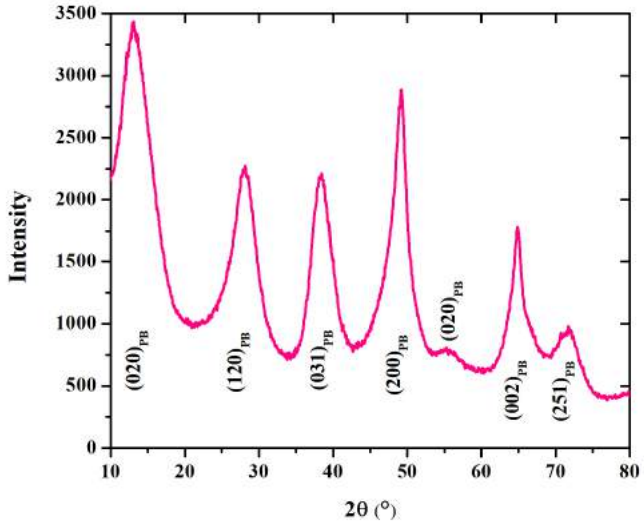

Figure 5.1: Characterization of the pseudoboehmite/aluminum substrate. XRD pattern of pseudoboehmite ($\gamma - AlO(OH)$).

Before silanization, atomic force microscopy (AFM) was used to check the roughness of the *Al-6063* surface after mechanical and electrochemical polishing. The AFM measurements (see Figure 5.2), show that before the electrochemical polish, the *Al-6063* had a surface roughness of $6.0 \pm 1.5nm$, while after the treatment, the roughness was of $1.5 \pm 0.24nm$. This allow that the NPs deposit could be at same level, and do not have zones with high difference height levels.

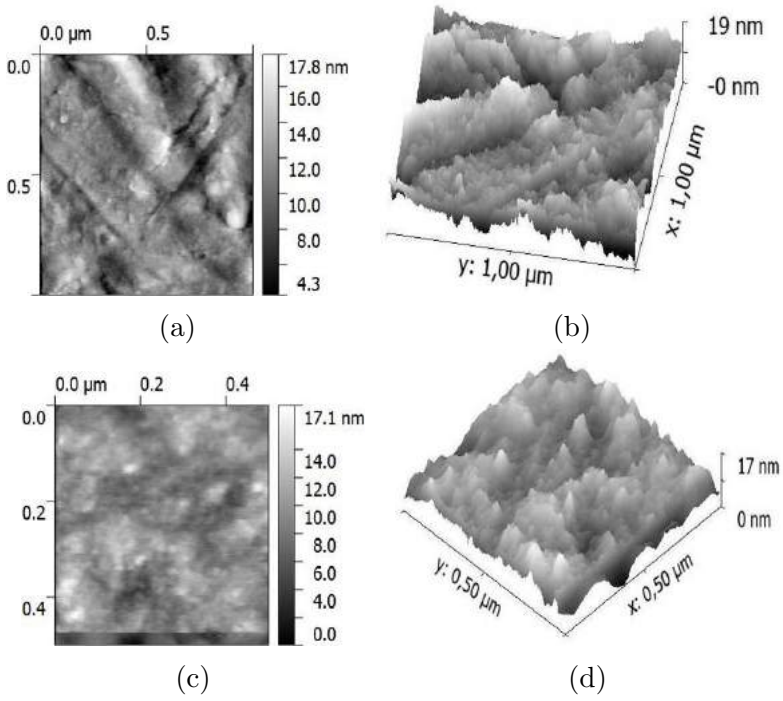

Figure 5.2: Atomic force microscopy (AFM) images of *Al-6063* slides after mechanical and electropolishing. **(a)**Two dimensional AFM image after mechanical polishing. **(b)**Three dimensional AFM image after mechanical polishing. **(c)**Two dimensional AFM image after electropolishing. **(d)**Three dimensional AFM image after electropolishing

The Al-substrate also was analysed by SEM, at a magnification of $350,000x$, working distance of $3.0mm$ and at a voltage of $15.0kV$. In Figure 5.3, the mesoporous surface due to the pseudoboehmite and the attached concave gold nanocubes (CGNC) can be seen. The functionalized surface of the Al slides allowed an homogeneous deposit of the CGNC.

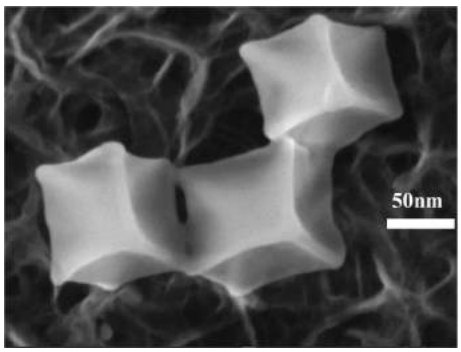

Figure 5.3: SEM image of pseudoboehmite/*Al-6063* substrate with some CGNC onto the pseudoboehmite.

5.2 Nanoparticles characterization

As was said in chapter 3.3, there are several ways to characterize the nanoparticles. In this work, the first analysis is the measurement of the UV-vis absorption spectra, and then the SEM analysis, to assure that the morphology is the desired one, and also, obtain the average size of the CGNC.

The variation of volume of seeds added to the growth solution lead to a variation in size of the nanoparticle. The main purpose of growing NPs with several sizes, was to find the best suitable nanocube that enhanced the Raman signal for single molecule detection application.

Seeds volume variation

To tune the size of the NPs, the volume of seeds that were added to the growth solution change. To a volume of $10mL$ of growth solution, $5, 10, 20, 40, 60$ and $90\mu L$ of seeds were added. The resultant solutions exhibit a color from from clear teal to navy blue, respectively. The solutions were left to settle for about $12h$, and then the absorption spectra was obtained, this is shown in Figure 5.4.

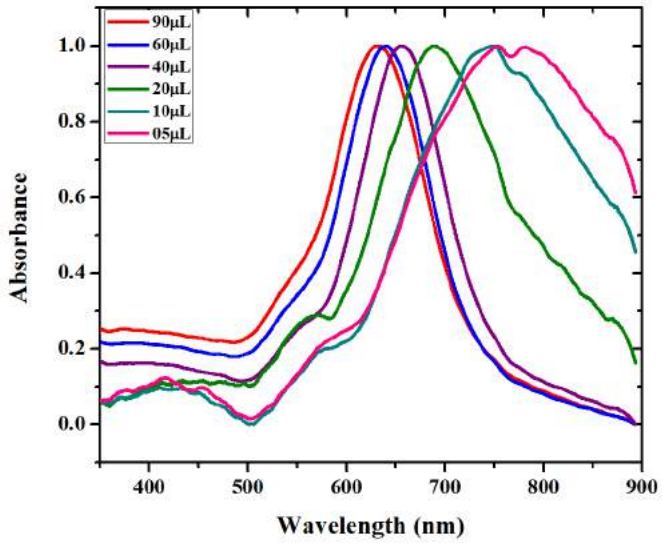

Figure 5.4: Absorbances of each one of the prepared solutions of CGNC. The bigger size (less added seeds) are shifter to the IR region.

The maximum absorbance peaks were at $631, 639, 655, 693, 747$ and $759nm$, strating with the $90\mu l$ volume seeds. From the absorbances figure, can be seen that the addition of small volumes of seeds leads to a red shift of the LSPR, also, a broadening in the peak, attributed to the formation of different morphology species (stars).

After the solutions were left in rest, were centrifugated at different rates for each solution. As was said before, this is an important step, since the CTAC is the one that gives stability to the nanoparticle, and remove it completely from the NP can induce their lost, but if the cleaning is not good, the remaining surfactant still can contribute to Raman signal.

Then, once the NPs are clean (centrifugated), SEM analysis was carried on (see Figure 5.5), at $100,000x, 15kV, and 3.0mm$ of working distance (WD). All the images were taken under the same conditions of work distance and voltage.

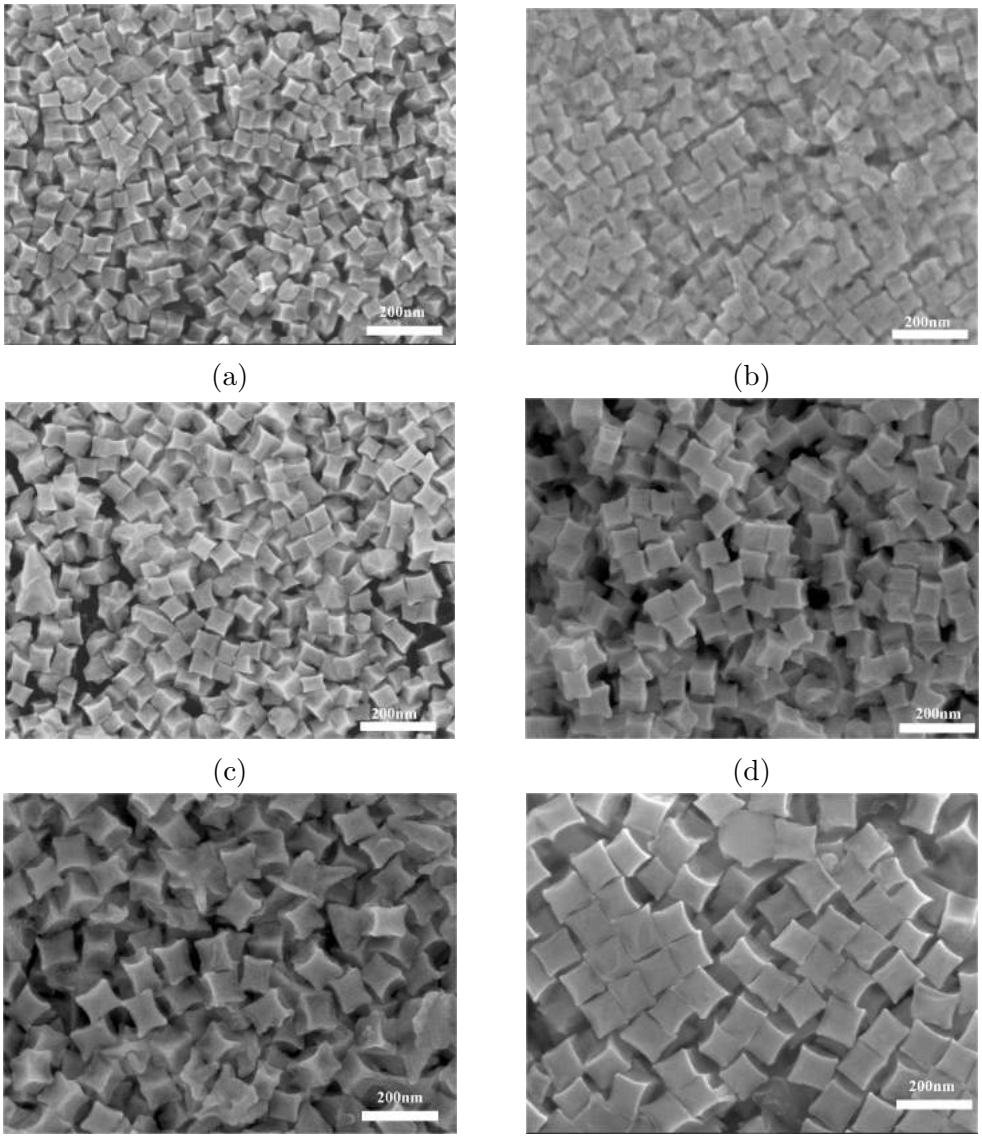

Figure 5.5: Micrography of the CGNCs. **(a)**$36 \pm 5nm$. **(b)**$42 \pm 5nm$. **(c)** $46 \pm 7nm$. **(d)**$55 \pm 9nm$. **(e)** $63 \pm 5nm$. **(f)**$85 \pm 8nm$.

The average size of gold nanocubes was measured by means of *ImageJ*. The mean sizes were from $36nm$ to $85nm$ for the case of $90\mu L$ and $5\mu L$ respectively.

From the graph in Figure 5.4, the data of the resulting nanoparticle size, the maximum absorption peak and the volume of seeds that was added were condensed in graph 5.6. From here an be seen that show a quadratic relation, showing the shift to the IR region.

Also, show the relation that exist between the NP size and the volume of added seeds, the bigger the volume added, the smaller the size of obtained nanoparticle.

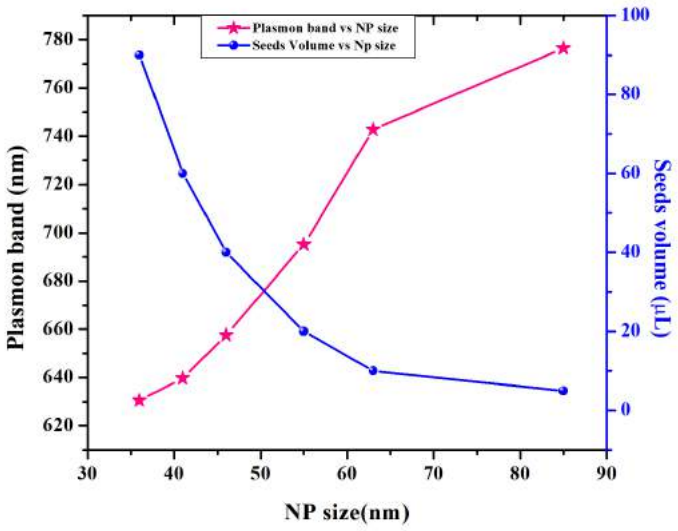

Figure 5.6: Plot of NP size vs Plasmon resonance in the left axis and *vs* Volume seeds added to growth solution at the right axis.

5.3 SERS analysis of CGNC.

A drop of $3\mu L$ of each size of the nanocubes was deposited on the surface of the electropolished *Al-6063* slide and left dry at room temperature (Figure 5.7a).

(a) (b)

Figure 5.7: Measurement conditions. **(a)**Deposit of CGNC of different sizes over the Al-substrate. **(b)**Scanning map to obtain the SERS measurements of 4-ATP

The molecule 4-aminothiophenol (4-ATP) was chosen as probe molecule, since this

molecule has a high effective section and its affinity with the gold nanoparticles due its thiol and amino functional groups. When the NPs drop was dried, a drop of $3\mu L$ of 4-ATP at a concentration of $1 \times 10^{-6} M$ was placed onto it, and let dry. Then the SERS spectra was obtained measuring over the NPs with 4-ATP dry drop.

The scans were obtained in eight different places of the dry drop, and 20 scans were measured in each place (see Figure 5.7b). All the measurements were taken with a *Renishaw InVia* microscope Raman spectrometer, with a excitation source at $\lambda = 785nm$, using a $20x$ objective ($0.4NA$) focused in the dry drop of CGNC, with $8mW$ of laser power at the exit, $1s$ of integration time and 20 accumulations.

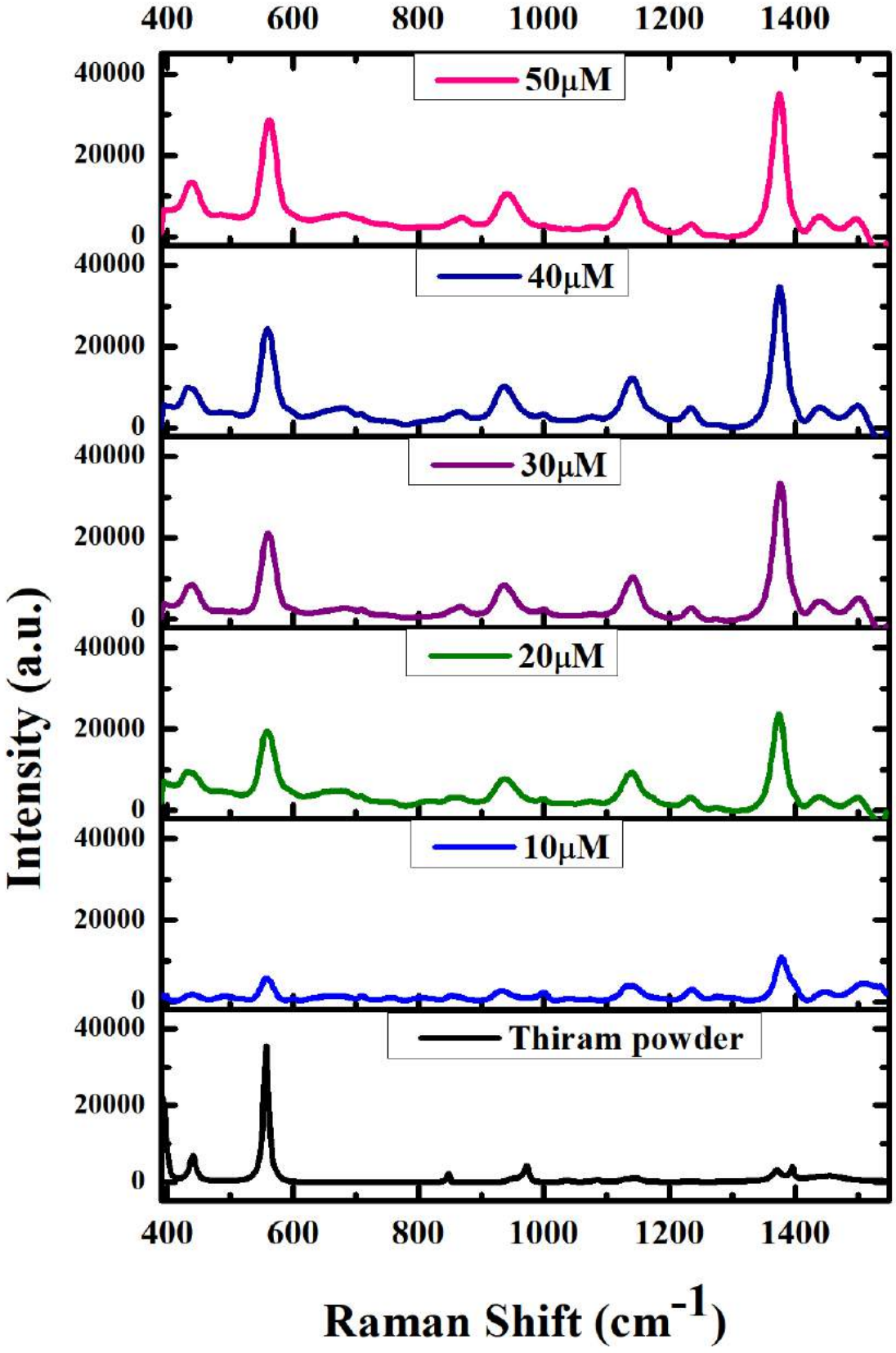

Figure 5.8: **(a)** Raman spectra of 4-ATP at $7.6M$ in ethanol. **(b)-(g)** SERS spectra of 4-ATP at 1.00×10^{-6} for the different volume of added seeds, from $90\mu l$ to $05\mu l$.

The average signal data was obtained for each NP size, and the peak intensity was compared in order to see which size was selected that showed the highest enhancement of the 4-ATP molecule (see figure. 5.8). As can be seen in Figure 5.8, there are four intense main peaks: $701, 1076, 1440, 1588 cm^{-1}$, consistent with the reports [113].

Two peaks were selected to observe the behaviour of the signal, $1075, 1588 cm^{-1}$, and show that the signal is higher for the $55nm$ CGNC size (see Figure 5.9). The graph shows the relation between the NP size and the peak intensity, as can be seen, the greatest enhancement was for the $55nm$ size, for both peaks.

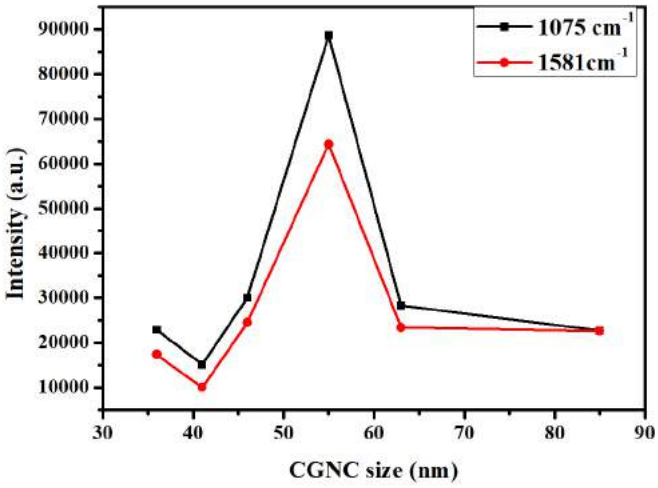

Figure 5.9: Graph of intensity peak vs CGNC size for the peaks $1076, 1588 cm^{-1}$

5.3.1 SERS sensor characterization : Rhodamine 6G, Crystal Violet and Rose Bengal Dyes.

Once the optimal nanocube size was determined, the probes with dyes were carried on. The SERS sensors were fabricated using the gold concave nanocubes of $55nm$. As was mentioned before the sensor was prepared by following the procedure described before (section 4.2). The CGNC were characterized by UV-vis spectroscopy (Figure 5.10) and

by SEM to confirm the morphology and size are the needed.

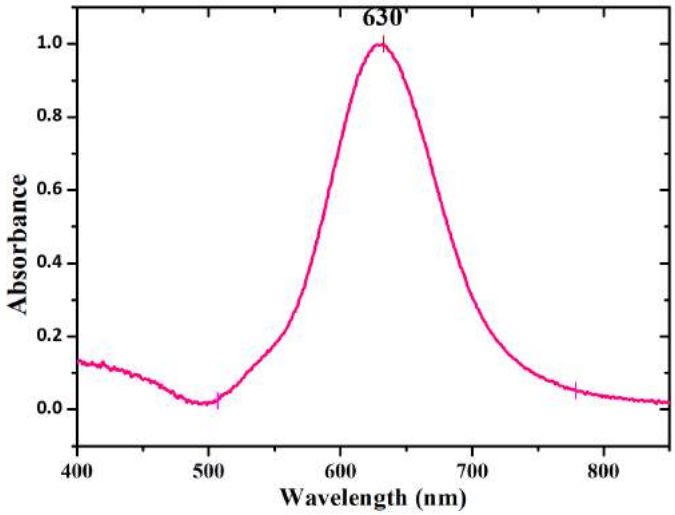

Figure 5.10: UV-vis absorbance spectrum of colloidal CGNC. The peak is localized at $630nm$.

The NPs were cleaned four times and concentrated to $10OD$. Two drops of the CGNC were deposited: first, a drop of $3\mu L$ is deposited and let dry at ambient conditions. Once that the first drop has dried, a second one was deposited over and waited to dry [32].

Different concentrations of Rhodamine6G (Rh6G) were prepared: $1 \times 10^{-3}, 1 \times 10^{-6}, 2.2 \times 10^{-7}, 2.2 \times 10^{-9}, 2.2 \times 10^{-11}$ and $2.2 \times 10^{-13} M$.

For SERS analysis, $3.5\mu l$ of each sample of Rh6G was dropped onto the substrate with a mean diameter of $1.5mm$. Raman spectra were immediately recorded by using the $20x$ microscope objective in the central part of the drop (as a wet sample); a rectangular mesh of 5×5 points with a distance of $33\mu m$ between adjacent neighbours resulted in 30 spectra acquired and total covering area of $21780\mu m^2$. All Rh6G samples were analyzed by triplicate using SERS substrates prepared on different days.

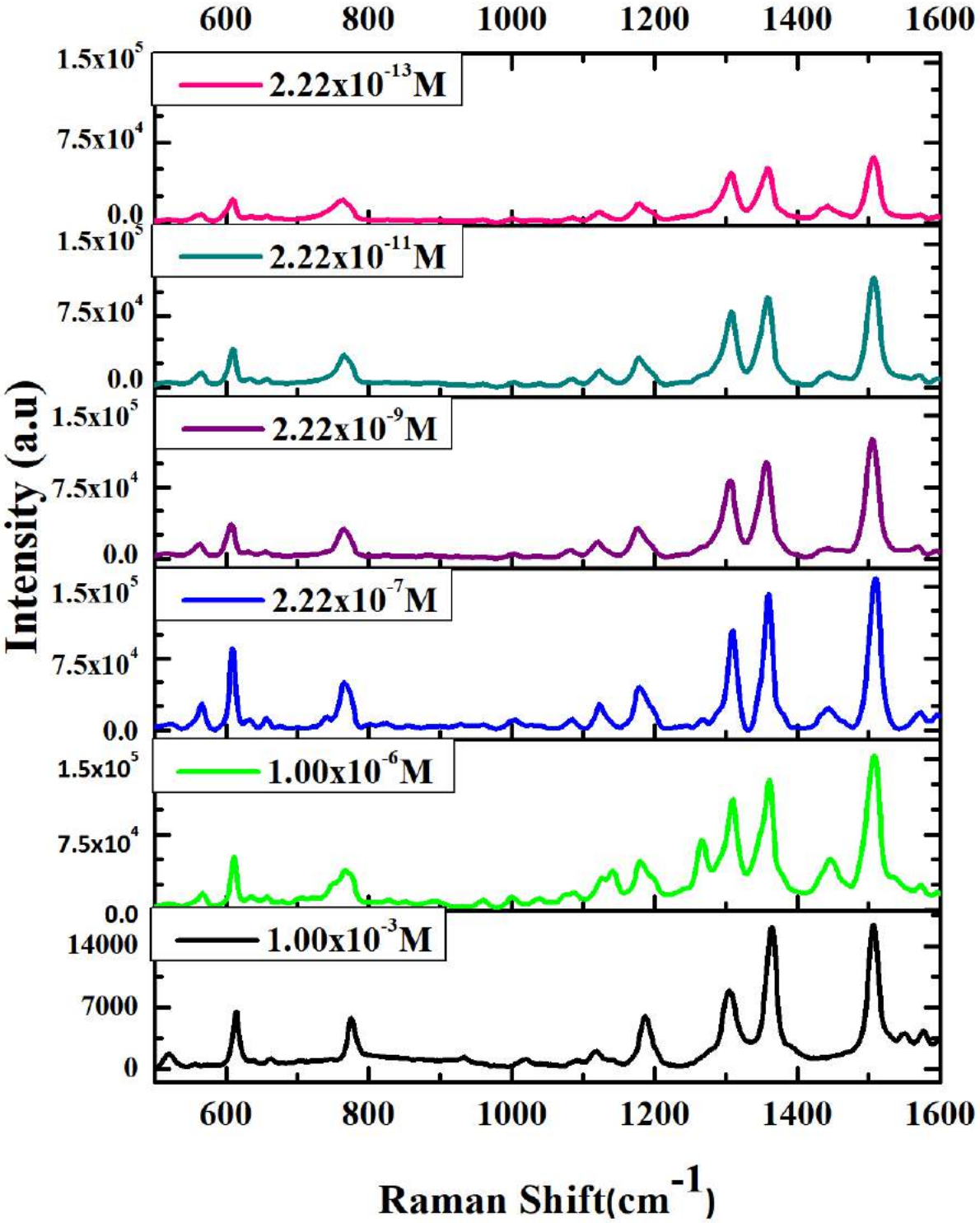

Figure 5.11: Average Raman SERS spectra of Rh6G measured on wet samples. **a)**Normal Raman spectrum of Rh6G on the *Al-APTS* surface without CGNC. **b-f)** SERS spectra of Rh6G samples onto the *Al-CGNC* substrate from $1.0 \times 10^{-6} M$ to $2.2 \times 10^{-13} M$.

The mean SERS spectrum for each concentration is shown in Figure 5.11, while the normal Raman spectrum of Rh6G on the Al-APTS surface without CGNCs is shown in Figure 5.11**(a)**. Five peaks of Rh6G were identified, and the corresponding band assignment is listed in Table 5.3. The peak located at $1508cm^{-1}$ (assigned to C-C stretching) was enhanced very strongly, followed by $11360cm^{-1}$ (assigned to aromatic ring C-C stretching) and $1309cm^{-1}$ (assigned to C-O-C stretching).

The good activity of the substrates, reproducibility and uniformity of SERS spectra is very important to evaluate the performance of the substrates as an analytical tool. To test the reproducibility of the SERS substrates, we prepared them three times on different days. The figure 5.12 shows a semi-Log plot of the SERS intensity of the Raman peak at $1508cm^{-1}$ as a function of molar concentration of Rh6G (from $1.00 \times 10^{-6}M$ to $2.22 \times 10^{-13}M$, all samples were measured in wet solution.

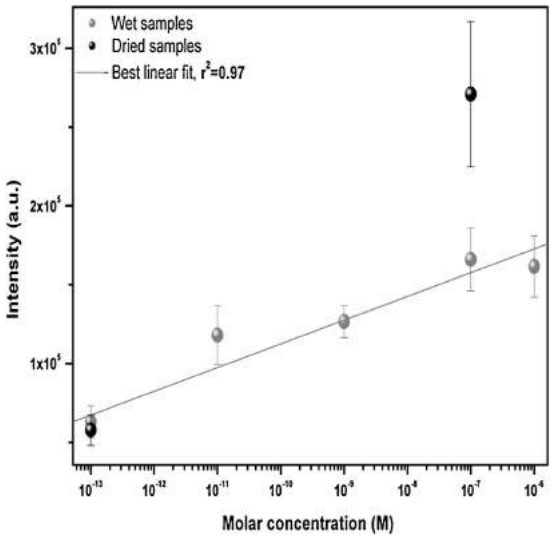

Figure 5.12: Semi-Log plot of SERS intensity at $1508cm^{-1}$ *vs* molar concentration of Rh6G. Each point represents the average value of the SERS signal from three different substrates, where the average value of each substrate was calculated using 30 spectra for each concentration.

The plot showed in Figure 5.12 confirm that SERS intensity exhibits a linear behavior as a function of Rh6G concentration; in the same figure, the error of the mean intensity

at $1508cm^{-1}$ is shown, and the error bars were calculated from the relative standard deviation (RSD), where the maximum calculated RSD was ≤ 0.12.The statistical analysis was carried out using all the recorded spectra acquired through automatic scanning, but they were acquired without an auto focused system.

These results show that our SERS substrates have a high capability of detection at lower molecular concentrations of Rh6G, almost in the order of submonolayer Rh6G concentration. One of the main advantages of our SERS substrates is that dry and wet analytes can be detected at low concentrations. On a second part, we tested the uniformity of the SERS signal once the samples of Rh6G were dry. For this analysis, we chose a rectangular mesh of 10×10 points, acquiring a total of 100 SERS spectra. Rh6G samples with concentrations of $1.00 \times 10^{-6}M$ and $2.22 \times 10^{-13}M$ were considered, representing maximum and minimum values analysed in the measurement of wet samples.

The figures 5.13a and 5.13c show the mapping images for both concentrations at the selected band for a total scanned area of $55 \times 75\mu m$. The mapping images reveal the variability in SERS signal intensity and thus allow to evaluate the uniformity of the Al-CGNC substrate; all the spectra used for the mapping were recorded automatically, but as it was mentioned before, the micro Raman system does not have an automatic focusing system.

Under these experimental conditions, the calculated RSD on the 100 spectra were 0.19 and 0.22 respectively for each case. The figures in 5.13b and 5.13d show 25 representative spectra from the automatic mapping of figures 5.13a and 5.13c.

Table 5.1: Parameters used for the calculation of the EF.

Spectra	Concentration (M)	Relative intensity		
		$1508cm^{-1}$	$1360cm^{-1}$	$611cm^{-1}$
SERS	2.22×10^{-13}	1.69×10^{5}	1.36×10^{5}	0.87×10^{5}
Raman	1.00×10^{-3}	2.35×10^{4}	2.47×10^{4}	1.10×10^{4}
	EF	6.40×10^{7}	4.90×10^{7}	7.03×10^{7}
	AEF	3.24×10^{10}	2.48×10^{10}	3.56×10^{10}

To quantify the SERS activity of the substrates, the enhancement factor (EF) was calculated using the acquired spectra from the dried samples. The EF was calculated by comparing the intensity of the minimum detected concentration of Rh6G from the SERS signal to that from the bulk Raman signal by means of the formula

$$EF = \frac{\frac{I_{SERS}}{N_{SERS}}}{\frac{I_{RS}}{N_{Vol}}} \tag{5.1}$$

where I_{SERS} and I_{Raman} are the intensities of the selected scattering bands in the SERS and bulk Raman spectra, while N_{SERS} and N_{Vol} are the number of probe molecules contributing to SERS and bulk Raman signals, respectively [72].

In both cases, we assume that molecules are distributed homogenously on the surface of the Al-CGNC substrate once the sample drop are dried; then, the number of probe molecules N_{Vol}, contributing to the signal, can be estimated by the following equation

$$N_{Vol} = N_{Avog} C_{Vol} A_{spot} h_{eff} \tag{5.2}$$

where N_{Avog} is Avogadro's number, C_{Vol} is the Rh6G concentration ($1.00 \times 10^{-3} M$), A_{spot} is the area of the laser spot ($4.9 \mu m^2$) and h_{eff} is the thickness of the focal spot

$(2.2\mu m)$.

While the number of molecules sampled in the SERS substrates, N_{SERS} was determined by following a similar methodology defined by Le Ru et al. and Orendorf et al. [72, 114].

$$N_{SERS} = \rho_{NP} A_{spot} A_{NP} N_{molec} \tag{5.3}$$

where ρ_{NP} is the number density of NPs $(156\frac{NPs}{\mu m^2})$, A_{NP} is the nanoparticle footprint area (concave nanocube,$(0.021\mu m^2)$, in this case the indented angle was $\sim 148^o$ [115] and N_{moles} is the density of Rh6G molecules bonded to the substrate $0.26 molecules/\mu m^2$ at a concentration of $2.22 \times 10^{-13} M$.

In our calculations, the mean peaks intensity located at $1508, 1360, 611 cm^{-1}$ were used to estimate the EF (see 5.1 and 5.13). Based on these parameters, the calculated Raman EFs for the above peaks were $6.4 \times 10^7, 1.9 \times 10^7$, and 7.0×10^7 respectively.

In table 5.1, the analytical enhancement factor (AEF) also is calculated, and as can be seen, the values are in the order of $\sim 10^{10}$, three magnitude orders above the EF calculated considering the molecules density and the nanoparticles involved i the measurement process.

Table 5.2: Resume of the main parameters of the Rh6G samples for its detection using the SERS substrates.

Sample	Concentration (M)	Molecules on the substrate	Number of molecules per μm^2
A1(Raman)	1.00×10^{-3}	2.11×10^{15}	—
A2(SERS)	1.00×10^{-6}	2.11×10^{12}	1.20×10^{6}
A3(SERS)	2.22×10^{-7}	4.68×10^{11}	2.65×10^{5}
A4(SERS)	2.22×10^{-9}	4.68×10^{9}	1.20×10^{3}
A5(SERS)	2.22×10^{-11}	4.68×10^{7}	26.5
A5(SERS)	2.22×10^{-13}	4.68×10^{5}	0.26

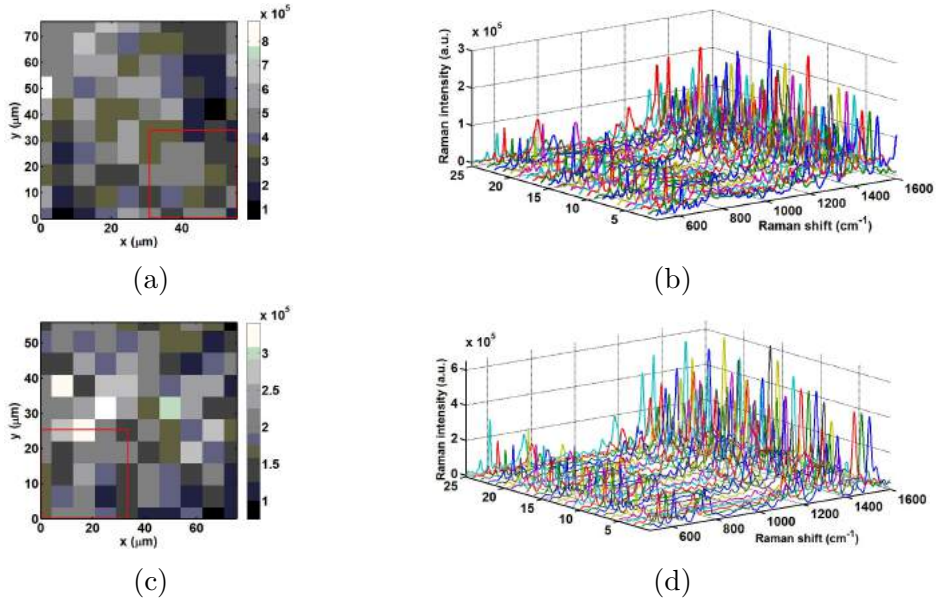

(a) (b)

(c) (d)

Figure 5.13: SERS analysis for the Rh6G $2.22 \times 10^{-13} M$ sample (top) and for $1.00 \times 10^{-6} M$.**(a)** Map image of the SERS intensity at $1508 cm^{-1}$ for a total area of $55\mu m \times 75\mu m$.**(b)**Raman spectra of the selected area in 5.13a. The RSD of this zone in $1508 cm^{-1}$ is 0.19. **(c)**Map image of the SERS intensity at $1508 cm^{-1}$ for a total area of $55\mu m \times 75\mu m$. **(d)**Raman spectra of the selected area in 5.13c. The RDS of this zone in $1508 cm^{-1}$ peak is 0.22.

With this work, is shown that the Al-substrate is able to detect Rh6G in the order 2.22×10^{-13} by using CGNC with a very smooth and hydrophobic surface, which led to improving the performance of the intrinsic properties of CGNC (nanoantennas). The high EF value obtained could be explained by the contribution of:

- the isolated concave surfaces
- the hot spots formed between the tips and the concave face, and
- between faces of cubes when they are face to face or when faces are shifted (tips or nanoantennas)

Zhang et al. showed that a Raman enhancement of the order of 10^6 can be obtained using isolated CGNCs, where main hot spots are localized on the cube tips [115].

More recently, Matteini et al. demonstrated that CGNCs can produce effective hot spots also at the face-face and face-corner sites once the cubes are self-assembled in monolayers and that the face-face locations can act as nanoholes for effective molecule entrapment and detection [116]. CGNCs have been shown to be very efficient as SERS substrates, and significant EF factors have been reported by depositing them onto the surface of solid supports like glass and Teflon. Also show with this work that, using a simple and reliable methodology, it is possible to make a detection of a submonolayer concentration of Rh6G with a mean EF in the order of $\sim 10^7$, which opens the possibility of a simple and reliable way of using these substrates for single molecule detection.

5.3.2 SERS sensor: the case of Rose Bengal and Crystal Violet

The study of the SERS activity of our substrates was carried out using Rh6G (as was detailed before), Rose Bengal (RB) and Crystal Violet (CV). Here, the performance of the substrates tested in RB and CV is show to prove the potential of the substrates in the detection of other molecules.

A stock solution of RB and CV (both $1.00 \times 10^{-2} M$ in methanol) were prepared and subsequently diluted to $1.00. \times 10^{-10} M$ and $1.00 \times 10^{-12} M$ in milli-Q water, for both cases respectively.

The figures 5.14 and 5.15 show the Raman spectra for the Crystal violet and Rose

Bengal molecules, in the graph of the bottom, is shown the Raman measurements, while in the top the SERS case is shown. Even at these low concentrations the Raman signals are easily detectable and the characteristic Raman peaks for each molecule are well defined.

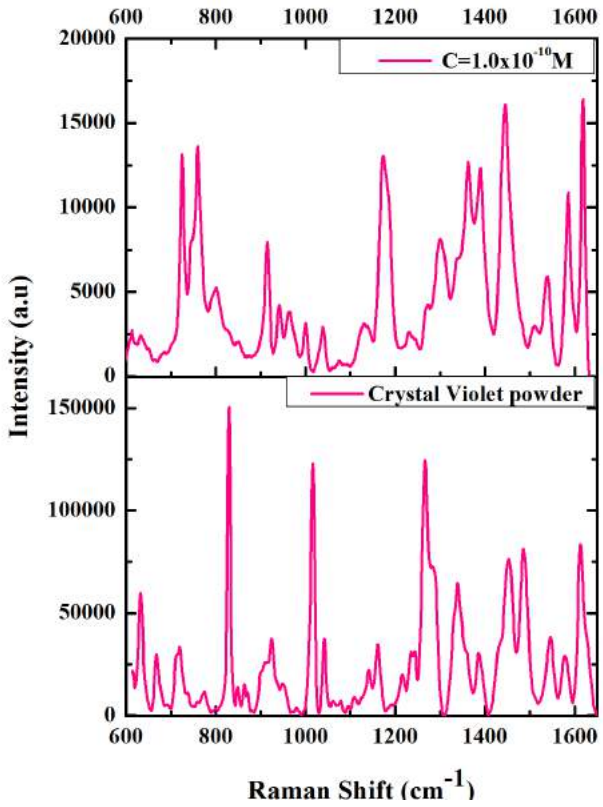

Figure 5.14: Raman and SERS spectra of Crystal Violet acquired as liquid samples at a concentration of $1.0 \times 10^{-2} M$ at the bottom and $1.0 \times 10^{-12} M$ at top. The high intensity SERS signal of Crystal Violet is listed in Table 5.3

.

Table 5.3: Band assignment for SERS spectra of Rh6G, crystal violet and rose bengal.

Rhodamine 6G		Crystal Violet		Rose Bengal	
SERS peak (cm^{-1})	Assignment	SERS peak (cm^{-1})	Assignment	SERS peak (cm^{-1})	Assignment
611	*ip* [1] C-C-C ring	724	νC-N[2]	724	–
1130	νC-H	760	$\nu C - C_{center}C$ / νC-N	724	—
1309	νC-O-C	1173	$\nu C - C_{center}C$	1350	ν(C-C)ring
1360	Arom νC-C	1445	δCH_3[3]	1438	—
1508	Arom νC-C, νC-H	1618	νArom C-C	—	—

[1] *in plane*

[2] *stretching*

[3] *scissoring*

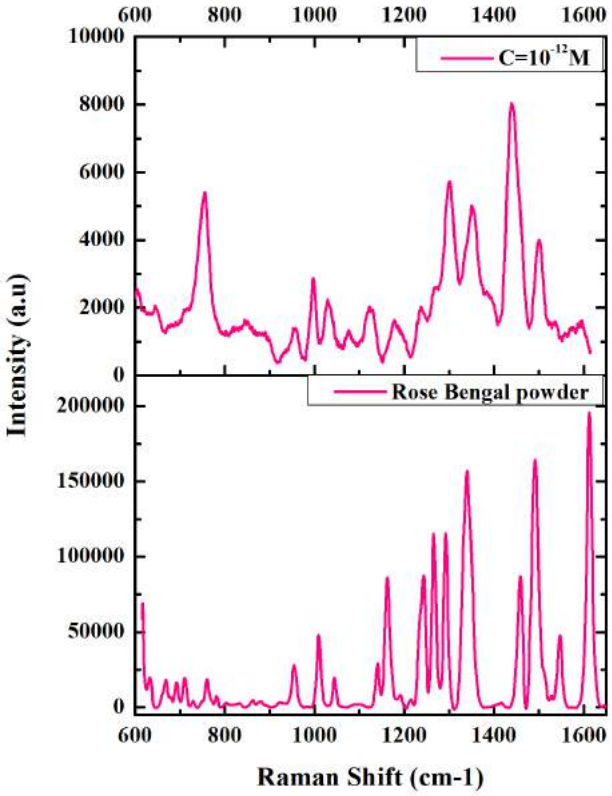

Figure 5.15: Raman and SERS spectra of Rose Bengal acquired as liquid samples at a concentration of $1.0 \times 10^{-3}M$ at the bottom and $1.0 \times 10^{-12}M$. The high intensity SERS signal is listed in Table 5.3

.

5.3.3 SERS Sensor: the case of pesticide Thiram

One of the objectives of this work was to being able to detect pesticides at very low concentrations by SERS, in the order of *ppm*. There are several works which aim is to detect the pesticide in values given by the farming government department, to show the potential of the technique. In this case, once that has been confirmed the optimal size of the CGNC for the best enhancement of Raman signal, and that can be achieved concentrations of $\sim 10^{-13}M$ on dyes, the Al substrate is proved for pesticides. In this case, the pesticide Thiram was chosen for the present study, due to the high affinity of

sulfur with gold metallic surface.

Thiram is a bisdithiocarbamate(EBDC) fungicide, used to prevent crop damage during the transportation or storage, as well as in the field (apples, peaches, and strawberries). Is applied to prevent fungal diseases as smut or bunts; also as repellent of rabbits, rodents and deer. Another use of thiram is in human scabies, as sunscreen and as bactericide [33, 117–119].

The substrates were prepared in the same way that is described in 5.3, and same size of CGNC ($\sim 55nm$). The NPs were also characterized by UV-Vis spectroscopy and by SEM.

A solution of thiram in methanol at $1 \times 10^{-2}M$ is prepared as stock solution, and also solutions of $50, 40, 30, 20$ and $10\mu M$ in water, upside and downside the permitted limits dictated by the EPA of $7ppm$ for apples [2]. A drop of the pesticide solution ($3\mu L$) is deposited over the dry nanoparticles, let dry and the SERS signal of the pesticide is measured for each one of the prepared concentrations. Eight different areas of the dry drop is measured, in order to have data about the uniformity of the signal.

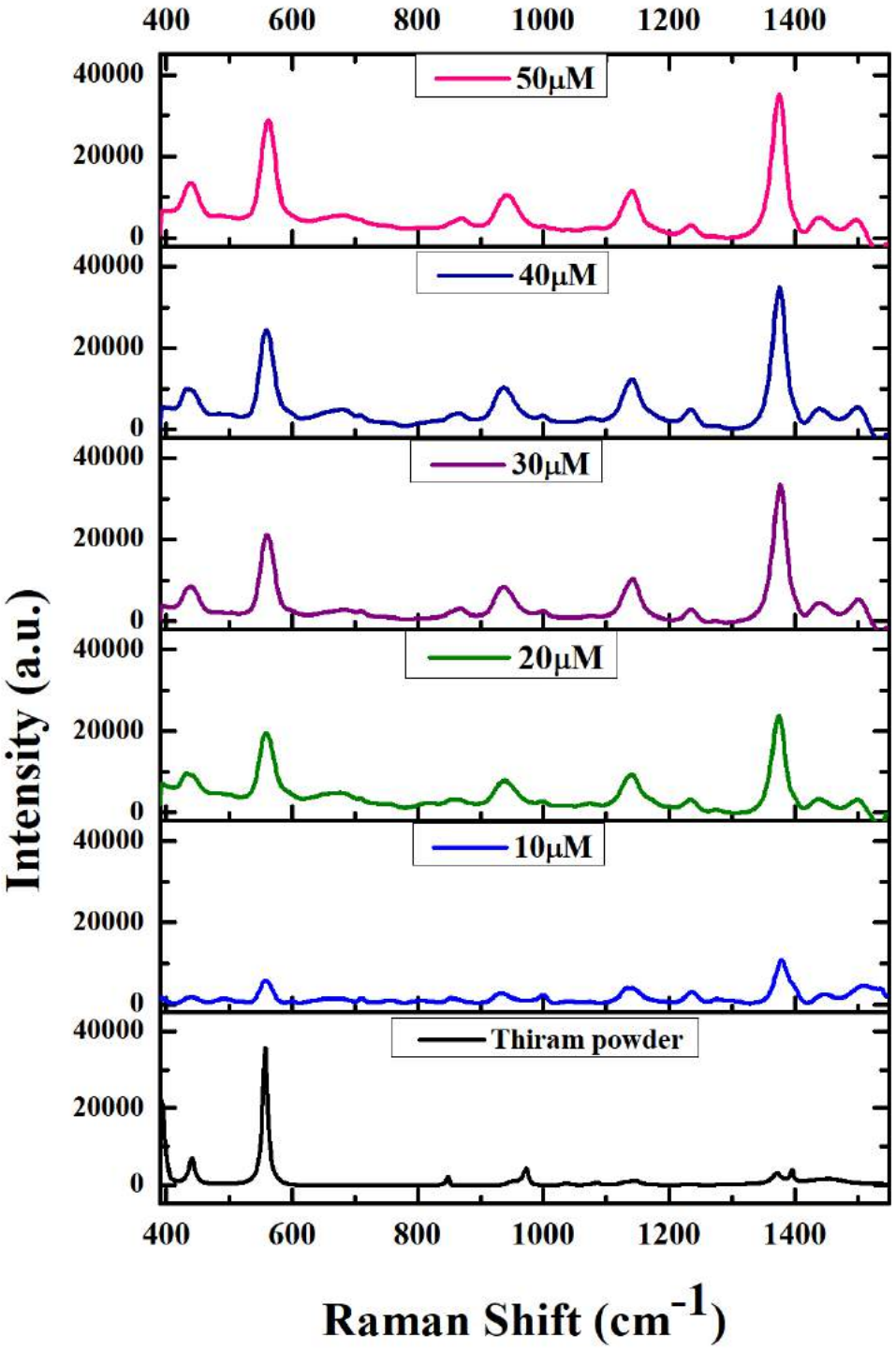

Figure 5.16: SERS spectra of thiram in powder and in concentrations from bottom to top of $50 - 10\mu M$.

In the figure 5.16, the signal of the Thiram in pure state (powder) is low, except for one peak in $557cm^{-1}$(attributed to $\nu(S-S)$), while in the SERS signal the rest of the peaks are clear, and even can be seen three peaks that are not so evident when the thiram is analysed as a powder . These peaks are $1140cm^{-1}$, corresponding to $\rho(CH_3)$ or $\nu C-N$, $1380cm^{-1}$ attributed to $\rho(CH_3)$ and 1510 to $\nu(C-N)$ [7, 27].

To prove the detection levels in fruits, a piece of tomato acquired from the local market, was blended with $20ml$ of milliQ water. Then, $1ml$ of the mixture was separated and $5\mu l$ of thiram pesticide at $20\mu M$ was added and mixed in the vortex. The solution was left in rest for about one hour and then was filtrated with filter paper. One drop of $5\mu l$ was taken and deposited over the SERS substrate and left dry.

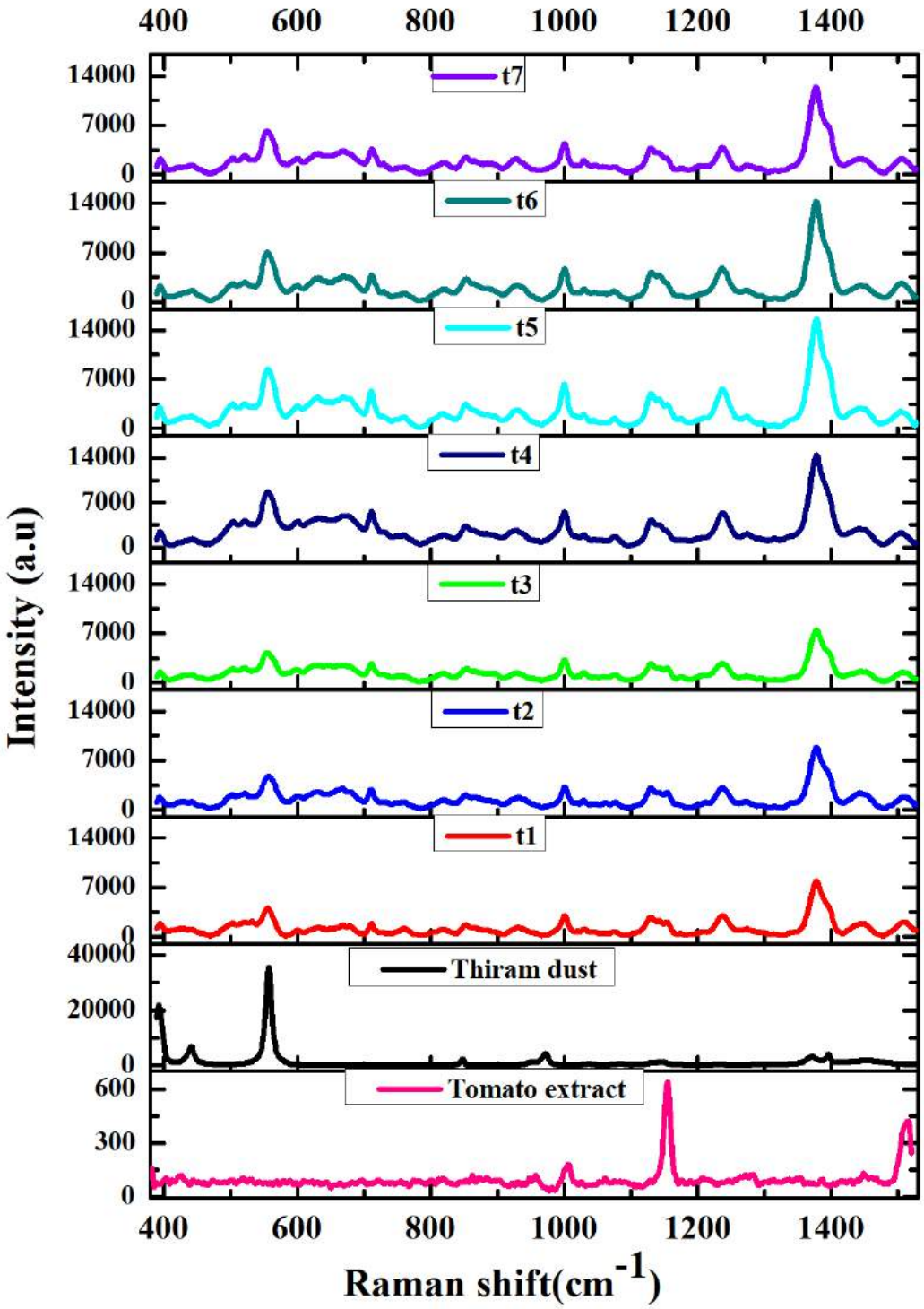

Figure 5.17: **(a)**Raman spectra of the thiram powder. **(b)-(h)** SERS spectra of the mixture of tomato with thiram.

The Raman spectra was obtained in seven different places of the dry drop of about $70 \times 70\mu m$, and in each place 20 spectra were taken, then the arithmetic media was obtained for each place. The seven spectra are showed in Figure 5.17, and in the bottom of the figure is the thiram powder spectra. Also, from the figure can be seen the peaks in $442, 555, 842, 1377$ and $1393 cm^{-1}$ peaks appear as in the thiram powder as in the mixture with tomato.

For the conducted tests, the lowest limit that could be detected with the substrate was $10\mu M$, below the limits established by the EPA. Also, the graph showed in Figure 5.17, is a proof of the potential of the technique and of the proposed SERS substrate for the study of pesticides in fruits and vegetables.

Chapter 6

Conclusions

This work presented the synthesis of concave gold nanocubes of different sizes and the fabrication of an aluminum substrate to study their performance in the enhancing of the Raman signal. In chapter 5 the nanoparticle synthesis is reported, as well as the changes made to synthesize nanocubes of different sizes, and the characterization made by UV-Vis spectroscopy and scanning electron microscopy (SEM) was used to analyze the size and morphology, reported in chapter 5.

In chapter 4, the process of polishing and functionalization of the aluminum substrate, while in chapter 5 is detailed the characterization of the substrate by atomic force microscopy (AFM), X-Ray diffraction (XRD) and SEM, to observe the grid that form the pseudoboehmite over the aluminum surface.

To characterize performance of the conjunction of the concave gold nanocubes plus the functionalized Al- substrate, first the optimal size of nanoparticles was proven. A series of NPs with different sizes was synthesized to measure the SERS signal of 4-aminothiophenol (4-atp). The sizes were $85, 63, 55, 46, 41$ and $36nm$, all of these were deposited by drop casting over the Al-substrate, and let dry. Then, a drop of 4-atp was deposited and the SERS signal was obtained. The signal in the main peaks was localized and, according to our results, the size that enhances the best, was of $\sim 55nm$.

Then, this size was tested by using dyes: Rhodamine 6G (Rh6G), Crystal Violet (CV) and Rose Bengal (RB) in limit concentrations of $2.22 \times 10^{-13}, 1.00 \times 10^{-10}, 1.00 \times 10^{-1} M$, respectively. The enhancement factor of the substrate with Rh6G was estimated, so it can be compared with others in the literature [72].

The tests made with the Al-substrate, showed a good performance for the deposit of nanoparticles, as well as good for SEM analysis, since allow a good image obtaining, not giving artifacts in the image due to the charge in the surface. Also, works as basis for SERS substrate, since do not give signal of fluorescence that opaque the Raman/SERS signal, allowing a good performance of the enhancing. Besides, the hydrophobic surface, allow that the deposit of the nanoparticles, could develop in an homogeneous way.

The tests made on pesticide Thiram, showed a good performance of the SERS substrate to amplify the signal of the analyte, open the possibility to use it as an alternative of the techniques used nowadays. Although there are a lot of work with pesticides and fruits,some of them only work with the fruit peel [23,120] and other with the fruit juice [8], the simple treatment of the samples and the use of the *Al-6063* basis, allow a better signal acquirement with no noise signal coming from it.

The preparation of the nanoparticles, as well as the characterization, and the probes made to assure the conjunction of the CGNC and the al-substrate are well suited for SERS.

The especial properties of the *Al-alloy* permits to avoid all those problems of fluorescence emission and Raman signal from solids like glass, paper or plastics, plus the expensive cost of silicon wafer. The combination of Al alloys and CGNC accounts for a strong enhancement of the SERS signal, being capable to detect Rh6G in the order of a sub-monolayer concentration ($10^{-13} M$) with an estimated EF of $\sim 10^7$.

.

Bibliography

[1] Sebastian Schlücker. *Surface-enhanced raman spectroscopy: Concepts and chemical applications*. Angewandte Chemie International Edition, 53(19):4756–4795, 2014.

[2] Enviromental Protection Authority. Pesticide use in nsw. http://www.epa.nsw.gov.au/your-environment/pesticides/pesticide-use-nsw, September 2017.

[3] National Institute of Enviromanetal Health Sciences. Pesticides. https://www.niehs.nih.gov/health/topics/agents/pesticides/index.cfm, August 2017.

[4] Wasim Aktar, Dwaipayan Sengupta, and Ashim Chowdhury. *Impact of pesticides use in agriculture: their benefits and hazards*. Interdisciplinary toxicology, 2(1):1–12, 2009.

[5] Shintaro Pang, Tianxi Yang, and Lili He. *Review of surface enhanced raman spectroscopic (sers) detection of synthetic chemical pesticides*. TrAC Trends in Analytical Chemistry, 85:73–82, 2016.

[6] Krongkamol Wong-Ek, Mati Horprathum, Pitak Eiamchai, Puenisara Limnonthakul, Viyapol Patthanasettakul, Pongpan Chindaudom, and Noppadon Nuntawong. Portable surface-enhanced raman spectroscopy for insecticide detection using silver nanorod film fabricated by magnetron sputtering. In *SPIE BiOS*, pages 791108–791108. International Society for Optics and Photonics, 2011.

[7] Chen Zhai, Yongyu Li, Yankun Peng, Tianfeng Xu, Sagar Dhakal, Kuanglin Chao, and Jianwei Qin. Research on identification and determination of mixed pesticides in apples using surface enhanced raman spectroscopy. In *SPIE Sensing Technology+ Applications*, pages 94880R–94880R. International Society for Optics and Photonics, 2015.

[8] Zhong Zhang, Qingsong Yu, Hao Li, Azlin Mustapha, and Mengshi Lin. *Standing gold nanorod arrays as reproducible sers substrates for measurement of pesticides in apple juice and vegetables*. Journal of food science, 80(2), 2015.

[9] Lei Ouyang, Wen Ren, Lihua Zhu, and Joseph Irudayaraj. *Prosperity to challenges: recent approaches in sers substrate fabrication*. Reviews in Analytical Chemistry, 36(1), 2017.

[10] Ying-Sing Li and Jeffrey S Church. *Raman spectroscopy in the analysis of food and pharmaceutical nanomaterials.* Journal of food and drug analysis, 22(1):29–48, 2014.

[11] Brian Bohunicky and Shaker A Mousa. *Biosensors: the new wave in cancer diagnosis.* Nanotechnology, science and applications, 4:1, 2011.

[12] Elena Mikhailovna Egorova, Aslan Amirkhanovich Kubatiev, and Vitaly Ivanovich Schvets. *Biological effects of metal nanoparticles.* Springer, 2016.

[13] Thuy-An Nguyen and Sang-Wha Lee. *Hierarchical au nanostructure electrodeposited on graphene oxide-modified ito glass as an ultrasensitive sers substrate.* Materials Research Bulletin, 83:550–555, 2016.

[14] Hiang Kwee Lee, Yih Hong Lee, In Yee Phang, Jiaqi Wei, Yue-E Miao, Tianxi Liu, and Xing Yi Ling. *Plasmonic liquid marbles: A miniature substrate-less sers platform for quantitative and multiplex ultratrace molecular detection.* Angewandte Chemie, 126(20):5154–5158, 2014.

[15] Ala M Alak and Tuan Vo-Dinh. *Surface-enhanced raman spectrometry of organo phosphorus chemical agents.* Analytical chemistry, 59(17):2149–2153, 1987.

[16] David A Armbruster and Terry Pry. *Limit of blank, limit of detection and limit of quantitation.* The Clinical Biochemist Reviews, 29(Suppl 1):S49, 2008.

[17] European Food Safety Authority. Pestcides, 2017.

[18] Anna A Semenova, Eugene A Goodilin, Nadezda A Brazhe, Vladimir K Ivanov, Alexander E Baranchikov, Vasiliy A Lebedev, Anastasia E Goldt, Olga V Sosnovtseva, Sergey V Savilov, Alexander V Egorov, et al. *Planar sers nanostructures with stochastic silver ring morphology for biosensor chips.* Journal of Materials Chemistry, 22(47):24530–24544, 2012.

[19] Xuemei Han, Hui Wang, Xuemei Ou, and Xiaohong Zhang. *Highly sensitive, reproducible, and stable sers sensors based on well-controlled silver nanoparticle-decorated silicon nanowire building blocks.* Journal of Materials Chemistry, 22(28):14127–14132, 2012.

[20] Benjamin Saute and Radha Narayanan. *Solution-based direct readout surface enhanced raman spectroscopic (sers) detection of ultra-low levels of thiram with dog-bone shaped gold nanoparticles.* Analyst, 136(3):527–532, 2011.

[21] Piersandro Pallavicini, Alice Dona, Angelo Taglietti, Paolo Minzioni, Maddalena Patrini, Giacomo Dacarro, Giuseppe Chirico, Laura Sironi, Nora Bloise, Livia Visai, et al. *Self-assembled monolayers of gold nanostars: a convenient tool for near-ir photothermal biofilm eradication.* Chemical Communications, 50(16):1969–1971, 2014.

[22] Bin Wang, Li Zhang, and Xia Zhou. *Synthesis of silver nanocubes as a sers substrate for the determination of pesticide paraoxon and thiram.* Spectrochimica Acta Part A: Molecular and Biomolecular Spectroscopy, 121:63–69, 2014.

[23] Pengzhen Guo, Debabrata Sikdar, Xiqiang Huang, Kae Jye Si, Wei Xiong, Shu Gong, Lim Wei Yap, Malin Premaratne, and Wenlong Cheng. *Plasmonic core–shell nanoparticles for sers detection of the pesticide thiram: size-and shape-dependent raman enhancement.* Nanoscale, 7(7):2862–2868, 2015.

[24] Kun Guo, Rui Xiao, Xiaoye Zhang, Chaoguang Wang, Qiqi Liu, Zhen Rong, Lin Ye, and Suhong Chen. *Silver nanopartical over aufon substrate for enhanced raman readout and their application in pesticide monitoring.* Molecules, 20(4):6299–6309, 2015.

[25] Jae-Soo Kang, Seon-Yeong Hwang, Chul-Jae Lee, and Mu-Sang Lee. *Sers of dithiocarbamate pesticides adsorbed on silver surface; thiram.* Bulletin of the Korean Chemical Society, 23(11):1604–1610, 2002.

[26] Jana Kubackova, Gabriela Fabriciova, Pavol Miskovsky, Daniel Jancura, and Santiago Sanchez-Cortes. *Sensitive surface-enhanced raman spectroscopy (sers) detection of organochlorine pesticides by alkyl dithiol-functionalized metal nanoparticles-induced plasmonic hot spots.* Analytical chemistry, 87(1):663–669, 2014.

[27] Yiqun Zhu, Minqiang Li, Daoyang Yu, and Liangbao Yang. *A novel paper rag as 'd-sers' substrate for detection of pesticide residues at various peels.* Talanta, 128:117–124, 2014.

[28] Yiqun Zhu, Li Zhang, and Liangbao Yang. *Designing of the functional paper-based surface-enhanced raman spectroscopy substrates for colorants detection.* Materials Research Bulletin, 63:199–204, 2015.

[29] Minsung Park, Hyejin Chang, Dae Hong Jeong, and Jinho Hyun. *Spatial deformation of nanocellulose hydrogel enhances sers.* BioChip Journal, 7(3):234–241, 2013.

[30] Li-Qiang Lu, Yin Zheng, Wen-Gang Qu, Han-Qing Yu, and An-Wu Xu. *Hydrophobic teflon films as concentrators for single-molecule sers detection.* Journal of Materials Chemistry, 22(39):20986–20990, 2012.

[31] Kristina Gudun, Zarina Elemessova, Laura Khamkhash, Ekaterina Ralchenko, and Rostislav Bukasov. *Commercial gold nanoparticles on untreated aluminum foil: Versatile, sensitive, and cost-effective sers substrate.* Journal of Nanomaterials, 2017, 2017.

[32] Pablo Genaro Martínez-Torres, Monica Monserrat Martínez-García, Pablo Eduado Cardoso-Ávila, and Juan Luis Pichardo-Molina. *Facile nanostructured substrate preparation using gold nanocuboids for sers.* Nanomaterials and Nanotechnology, 5:12, 2015.

[33] Boris N. Khlebtsov, Vitaly A. Khanadeev, Elizaveta V. Panfilova, Daniil N. Bratashov, and Nikolai G. Khlebtsov. *Gold nanoisland films as reproducible sers substrates for highly sensitive detection of fungicides.* ACS Applied Materials & Interfaces, 7(12):6518–6529, 2015.

[34] Wisiani Wijaya, Shintaro Pang, Theodore P Labuza, and Lili He. *Rapid detection of acetamiprid in foods using surface-enhanced raman spectroscopy (sers).* Journal of food science, 79(4), 2014.

[35] Yande Liu and Tao Liu. Determination of pesticide residues on the surface of fruits using micro-raman spectroscopy. In *International Conference on Computer and Computing Technologies in Agriculture*, pages 427–434. Springer, 2010.

[36] Eric Lichtfouse. Nanoscience in food and agriculture 3, 2016.

[37] Heather J Bowley, Don L Gerrard, John D Louden, and George Turrell. *Practical Raman spectroscopy.* Springer Science & Business Media, 2012.

[38] Colm P O'Donnell, Colette Fagan, and Patrick J Cullen. *Process analytical technology for the food industry.* Springer, 2014.

[39] Ewen Smith and Geoffrey Dent. *Modern Raman spectroscopy: a practical approach.* John Wiley & Sons, 2013.

[40] Anette Müllertz, Yvonne Perrie, and Thomas Rades. *Analytical Techniques in the Pharmaceutical Sciences.* Springer, 2016.

[41] Tigran V Shahbazyan and Mark I Stockman. *Plasmonics: theory and applications.* Springer, 2013.

[42] John R Ferraro. *Introductory Raman spectroscopy.* Academic press, 2003.

[43] Derek A Long. *The raman effect: a unified treatment of the theory of raman scattering by molecules.* West Sussex, 2002.

[44] Christy L Haynes, Adam D McFarland, and Richard P Van Duyne. Surface-enhanced raman spectroscopy, 2005.

[45] Rolf Schäfer and Peter C Schmidt. *Methods in physical chemistry.* John Wiley & Sons, 2012.

[46] Anette Müllertz, Yvonne Perrie, and Thomas Rades. *Analytical Techniques in the Pharmaceutical Sciences.* Springer, 2016.

[47] DR Vij. *Handbook of applied solid state spectroscopy.* Springer Science & Business Media, 2007.

[48] P.S. Sindhu. *Fundamentals of Molecular Spectroscopy.* New Age International (P) Limited, 2006.

[49] Marek Procházka. *Surface-enhanced raman spectroscopy.* Biological and Medical Physics, Biomedical Engineering, 2016.

[50] Katrin Kneipp, Harald Kneipp, and Janina Kneipp. Plasmonics for enhanced vibrational signatures. In *Plasmonics: Theory and Applications*, pages 103–124. Springer, 2013.

[51] Dixit N Sathyanarayana. *Vibrational spectroscopy: theory and applications.* New Age International, 2015.

[52] D.C. Dash. *Analytical Chemistry.* PHI Learning, 2011.

[53] Katrin Kneipp, Harald Kneipp, Irving Itzkan, Ramachandra R Dasari, and Michael S Feld. *Surface-enhanced raman scattering and biophysics.* Journal of Physics: Condensed Matter, 14(18):R597, 2002.

[54] Martin Fleischmann, Patrick J Hendra, and A James McQuillan. *Raman spectra of pyridine adsorbed at a silver electrode.* Chemical Physics Letters, 26(2):163–166, 1974.

[55] David L Jeanmaire and Richard P Van Duyne. *Surface raman spectroelectrochemistry: Part i. heterocyclic, aromatic, and aliphatic amines adsorbed on the anodized silver electrode.* Journal of Electroanalytical Chemistry and Interfacial Electrochemistry, 84(1):1–20, 1977.

[56] M Moskkovits and H Knepp. Surface enhanced raman scattering–physics and applications, 2010.

[57] Alan Campion and Patanjali Kambhampati. *Surface-enhanced raman scattering.* Chemical society reviews, 27(4):241–250, 1998.

[58] Tuan Vo-Dinh. *Surface-enhanced raman spectroscopy using metallic nanostructures.* TrAC Trends in Analytical Chemistry, 17(8):557–582, 1998.

[59] Jordan F Betz, W Yu Wei, Yi Cheng, Ian M White, and Gary W Rubloff. *Simple sers substrates: powerful, portable, and full of potential.* Physical Chemistry Chemical Physics, 16(6):2224–2239, 2014.

[60] David P Fromm, Arvind Sundaramurthy, Anika Kinkhabwala, P James Schuck, Gordon S Kino, and WE Moerner. Exploring the chemical enhancement for surface-enhanced raman scattering with au bowtie nanoantennas, 2006.

[61] Hans-Eckhardt Schaefer. *Nanoscience: the science of the small in physics, engineering, chemistry, biology and medicine.* Springer Science & Business Media, 2010.

[62] JM Romo-Herrera, AL González, L Guerrini, FR Castiello, G Alonso-Nuñez, OE Contreras, and RA Alvarez-Puebla. *Correction: A study of the depth and size of concave cube au nanoparticles as highly sensitive sers probes.* Nanoscale, 9(15):5020–5020, 2017.

[63] Qiang Zhang, Yufeng Yuan, Changping Wang, Zhengjie Zhou, Li Li, Sanjun Zhang, and Jianhua Xu. *Design considerations for sers detection in colloidal solution: reduce spectral intensity fluctuation.* Journal of Raman Spectroscopy, 47(4):395–401, 2016.

[64] Miguel A García. *Surface plasmons in metallic nanoparticles: fundamentals and applications.* Journal of Physics D: Applied Physics, 44(28):283001, 2011.

[65] MA Mahmoud, B Snyder, and MA El-Sayed. *Surface plasmon fields and coupling in the hollow gold nanoparticles and surface-enhanced raman spectroscopy. theory and experiment.* The Journal of Physical Chemistry C, 114(16):7436–7443, 2010.

[66] George C Schatz and Richard P Van Duyne. *Electromagnetic mechanism of surface-enhanced spectroscopy.* Handbook of vibrational spectroscopy, 2002.

[67] Mamdouh E Abdelsalam, Sumeet Mahajan, Philip N Bartlett, Jeremy J Baumberg, and Andrea E Russell. *Sers at structured palladium and platinum surfaces.* Journal of the American chemical society, 129(23):7399–7406, 2007.

[68] Marie-Christine Daniel and Didier Astruc. *Gold nanoparticles: assembly, supramolecular chemistry, quantum-size-related properties, and applications toward biology, catalysis, and nanotechnology.* Chemical reviews, 104(1):293–346, 2004.

[69] Peter N Njoki, I-Im S Lim, Derrick Mott, Hye-Young Park, Bilal Khan, Suprav Mishra, Ravishanker Sujakumar, Jin Luo, and Chuan-Jian Zhong. *Size correlation of optical and spectroscopic properties for gold nanoparticles.* The Journal of Physical Chemistry C, 111(40):14664–14669, 2007.

[70] George Schatz, Matthew Young, and Richard Van Duyne. *Electromagnetic mechanism of sers.* Surface-enhanced Raman scattering, pages 19–45, 2006.

[71] Antonio Fernandez-Barbero, Rafael Contreras-Caceres, and Benjamin Sierra-Martin. Surface-enhanced raman scattering sensors based on hybrid nanoparticles. In Oleg Minin, editor, *Microsensors*, chapter 7. InTech, Rijeka, 2011.

[72] EC Le Ru, E Blackie, Matthias Meyer, and Pablo G Etchegoin. *Surface enhanced raman scattering enhancement factors: a comprehensive study.* The Journal of Physical Chemistry C, 111(37):13794–13803, 2007.

[73] Yanqin Cao, Junwei Zhang, Yong Yang, Zhengren Huang, Nguyen Viet Long, and Chaoli Fu. *Engineering of sers substrates based on noble metal nanomaterials for chemical and biomedical applications.* Applied Spectroscopy Reviews, 50(6):499–525, 2015.

[74] Lu-Bin Zhong, Jun Yin, Yu-Ming Zheng, Qing Liu, Xiao-Xia Cheng, and Fang-Hong Luo. *Self-assembly of au nanoparticles on pmma template as flexible, transparent, and highly active sers substrates.* Analytical chemistry, 86(13):6262–6267, 2014.

[75] Jon A Dieringer, Adam D McFarland, Nilam C Shah, Douglas A Stuart, Alyson V Whitney, Chanda R Yonzon, Matthew A Young, Xiaoyu Zhang, and Richard P Van Duyne. *Introductory lecture surface enhanced raman spectroscopy: new materials, concepts, characterization tools, and applications.* Faraday discussions, 132:9–26, 2006.

[76] Samuel E Lohse and Catherine J Murphy. *Applications of colloidal inorganic nanoparticles: from medicine to energy.* Journal of the American Chemical Society, 134(38):15607–15620, 2012.

[77] Ruyi Shi, Xiangjiang Liu, and Yibin Ying. *Facing challenges in real-life application of surface-enhanced raman scattering: Design and nanofabrication of surface-enhanced raman scattering substrates for rapid field test of food contaminants.* Journal of agricultural and food chemistry, 2017.

[78] Xia Zhou, Fei Zhou, Honglin Liu, Liangbao Yang, and Jinhuai Liu. *Assembly of polymer–gold nanostructures with high reproducibility into a monolayer film sers substrate with 5 nm gaps for pesticide trace detection.* Analyst, 138(19):5832–5838, 2013.

[79] Virginia Joseph, Andrea Matschulat, Jörg Polte, Simone Rolf, Franziska Emmerling, and Janina Kneipp. *Sers enhancement of gold nanospheres of defined size.* Journal of Raman Spectroscopy, 42(9):1736–1742, 2011.

[80] Benjamin Saute, Ranjith Premasiri, Lawrence Ziegler, and Radha Narayanan. *Gold nanorods as surface enhanced raman spectroscopy substrates for sensitive and selective detection of ultra-low levels of dithiocarbamate pesticides.* Analyst, 137(21):5082–5087, 2012.

[81] Sara E Skrabalak, Leslie Au, Xingde Li, and Younan Xia. *Facile synthesis of ag nanocubes and au nanocages.* Nature protocols, 2(9):2182–2190, 2007.

[82] Jin-Kyoung Yang, Homan Kang, Hyunmi Lee, Ahla Jo, Sinyoung Jeong, Su-Ji Jeon, Hye-In Kim, Ho-Young Lee, Dae Hong Jeong, Jong-Ho Kim, et al. *Single-step and rapid growth of silver nanoshells as sers-active nanostructures for label-free detection of pesticides.* ACS applied materials & interfaces, 6(15):12541–12549, 2014.

[83] Dana Cialla, Anne März, René Böhme, Frank Theil, Karina Weber, Michael Schmitt, and Jürgen Popp. *Surface-enhanced raman spectroscopy (sers): progress and trends.* Analytical and bioanalytical chemistry, 403(1):27–54, 2012.

[84] Vicky V Mody, Rodney Siwale, Ajay Singh, and Hardik R Mody. *Introduction to metallic nanoparticles.* Journal of Pharmacy and Bioallied Sciences, 2(4):282, 2010.

[85] Robert Vajtai. *Springer handbook of nanomaterials.* Springer Science & Business Media, 2013.

[86] Matthew M Bower, Christopher J DeSantis, and Sara E Skrabalak. *A quantitative analysis of anions and ph on the growth of bimetallic nanostructures.* The Journal of Physical Chemistry C, 118(32):18762–18770, 2014.

[87] P Zijlstra and M Orrit. *Single metal nanoparticles: optical detection, spectroscopy and applications.* Reports on Progress in Physics, 74(10):106401, 2011.

[88] Celso de Mello Donegá. *Nanoparticles: Workhorses of Nanoscience.* Springer, 2014.

[89] Elena Mikhailovna Egorova, Aslan Amirkhanovich Kubatiev, and Vitaly Ivanovich Schvets. *Biological effects of metal nanoparticles.* Springer, 2016.

[90] Hongbo Chen, Yi Zheng, Ge Tian, Yan Tian, Xiaowei Zeng, Gan Liu, Kexin Liu, Lei Li, Zhen Li, Lin Mei, et al. *Oral delivery of dmab-modified docetaxel-loaded plga-tpgs nanoparticles for cancer chemotherapy.* Nanoscale Res Lett, 6(1):4, 2011.

[91] James E Morris. Nanopackaging: nanotechnologies and electronics packaging. In *High Density Microsystem Design and Packaging and Component Failure Analysis, 2006. HDP'06. Conference on*, pages 199–205. IEEE, 2006.

[92] BS Murty, P Shankar, Baldev Raj, BB Rath, and James Murday. *Textbook of nanoscience and nanotechnology.* Springer Science & Business Media, 2013.

[93] Anatolii D Pomogailo and Gulzhian I Dzhardimalieva. *Nanostructured materials preparation via condensation ways.* Springer, 2016.

[94] Peter Baláž. Selected identification methods. In *Mechanochemistry in nanoscience and minerals engineering*, pages 133–175. Springer, 2008.

[95] Emilio I Alarcon, May Griffith, and Klas I Udekwu. *Silver Nanoparticle Applications.* Springer, 2015.

[96] Andrea R Tao, Susan Habas, and Peidong Yang. *Shape control of colloidal metal nanocrystals.* small, 4(3):310–325, 2008.

[97] Yue Yu, Qingbo Zhang, Xianmao Lu, and Jim Yang Lee. *Seed-mediated synthesis of monodisperse concave trisoctahedral gold nanocrystals with controllable sizes.* The Journal of Physical Chemistry C, 114(25):11119–11126, 2010.

[98] PE Cardoso-Avila, JL Pichardo-Molina, C Murali Krishna, and R Castro-Beltran. *Photochemical transformation of silver nanoparticles by combining blue and green irradiation.* Journal of Nanoparticle Research, 17(3):160, 2015.

[99] Saurabh Bhatia. *Natural Polymer Drug Delivery Systems: Nanoparticles, Plants, and Algae.* Springer, 2016.

[100] Robert Eisenthal and Michael J Danson. *Enzyme assays: a practical approach.* Number 257. Practical Approach (Paperback), 2002.

[101] Kourosh Kalantar-zadeh and Benjamin Fry. *Nanotechnology-enabled sensors*. Springer Science & Business Media, 2007.

[102] Jian Zhang, Mark R Langille, Michelle L Personick, Ke Zhang, Shuyou Li, and Chad A Mirkin. *Concave cubic gold nanocrystals with high-index facets*. Journal of the American Chemical Society, 132(40):14012–14014, 2010.

[103] Andrew R Markelonis, Joanna S Wang, Bruno Ullrich, Chien M Wai, and Gail J Brown. *Nanoparticle film deposition using a simple and fast centrifuge sedimentation method*. Applied Nanoscience, 5(4):457–468, 2015.

[104] Pablo Genaro Martínez-Torres, Monica Monserrat Martínez-García, Pablo Eduado Cardoso-Ávila, and Juan Luis Pichardo-Molina. *Facile nanostructured substrate preparation using gold nanocuboids for sers*. Nanomaterials and Nanotechnology, 5:12, 2015.

[105] Xiaohong Jiang, Min Yang, Yanjing Meng, Wei Jiang, and Jinhua Zhan. *Cysteamine-modified silver nanoparticle aggregates for quantitative sers sensing of pentachlorophenol with a portable raman spectrometer*. ACS applied materials & interfaces, 5(15):6902–6908, 2013.

[106] Andraz Kocjan, Ales Dakskobler, and Tomaz Kosmac. *Superhydrophobic nanostructured boehmite coatings prepared by aln powder hydrolysis*. International Journal of Applied Ceramic Technology, 8(4):848–853, 2011.

[107] Tatsuya Masuda, Hidetaka Asoh, Satoshi Haraguchi, and Sachiko Ono. *Fabrication and characterization of single phase α-alumina membranes with tunable pore diameters*. Materials, 8(3):1350–1368, 2015.

[108] Rameez Ud Din, Nikolaos Nikogeorgos, Morten Stendahl Jellesen, Rajashekhar Shabadi, and Rajan Ambat. *Influence of steam-based pre-treatment using acidic chemistries on the adhesion performance of powder coated aluminium alloy aa6060*. International Journal of Adhesion and Adhesives, 74:167–176, 2017.

[109] Di Ma, Shuying Li, and Chenghao Liang. *Electropolishing of high-purity aluminium in perchloric acid and ethanol solutions*. Corrosion Science, 51(4):713–718, 2009.

[110] WP Vellinga, G Eising, FM de Wit, JMC Mol, H Terryn, JHW de Wit, and J Th M De Hosson. *Adhesion at al-hydroxide-polymer interfaces: Influence of chemistry and evidence for microscopic self-pinning*. Materials Science and Engineering: A, 527(21):5637–5647, 2010.

[111] Min Hyung Lee, Namsoo Lim, Daniel J Ruebusch, Arash Jamshidi, Rehan Kapadia, Rebecca Lee, Tae Joon Seok, Kuniharu Takei, Kee Young Cho, Zhiyoung Fan, et al. *Roll-to-roll anodization and etching of aluminum foils for high-throughput surface nanotexturing*. Nano letters, 11(8):3425–3430, 2011.

[112] KI Shefer, DA Yatsenko, SV Tsybulya, ÉM Moroz, and E Yu Gerasimov. *Structural features of finely dispersed pseudoboehmite obtained by a sol-gel method.* Journal of Structural Chemistry, 51(2):322–326, 2010.

[113] Xiaoge Hu, Tie Wang, Liang Wang, and Shaojun Dong. *Surface-enhanced raman scattering of 4-aminothiophenol self-assembled monolayers in sandwich structure with nanoparticle shape dependence: off-surface plasmon resonance condition.* The Journal of Physical Chemistry C, 111(19):6962–6969, 2007.

[114] Christopher J Orendorff, Anand Gole, Tapan K Sau, and Catherine J Murphy. *Surface-enhanced raman spectroscopy of self-assembled monolayers: sandwich architecture and nanoparticle shape dependence.* Analytical chemistry, 77(10):3261–3266, 2005.

[115] Qingfeng Zhang, Nicolas Large, and Hui Wang. *Gold nanoparticles with tipped surface structures as substrates for single-particle surface-enhanced raman spectroscopy: concave nanocubes, nanotrisoctahedra, and nanostars.* ACS applied materials & interfaces, 6(19):17255–17267, 2014.

[116] Paolo Matteini, Marella de Angelis, Lorenzo Ulivi, Sonia Centi, and Roberto Pini. *Concave gold nanocube assemblies as nanotraps for surface-enhanced raman scattering-based detection of proteins.* Nanoscale, 7(8):3474–3480, 2015.

[117] Oregon State University Cooperative Extension Offices of Cornell University, Michigan State University and University of California at Davis. Pesticide information profile: Thiram.

[118] Bayer Global. Thiram.

[119] National Pesticide Information Center. Epa r.e.d facts: thiram, 2004.

[120] Yingcheng Wang, Yuanhao Jin, Xiaoyang Xiao, Tianfu Zhang, Haitao Yang, Yudan Zhao, Jiaping Wang, Kaili Jiang, Shoushan Fan, and Qunqing Li. *Flexible, transparent and highly sensitive sers substrates with cross-nanoporous structures for fast on-site detection.* Nanoscale, 2018.